Activity-dependent Sonic hedgehog signaling promotes astrocyte modulation of synaptic plasticity

Anh Duc Le[1], Marissa Fu[1], Riya Kumar[1], Gloria Zacharias[1], A. Denise R. Garcia[2]

[1]Department of Biology, Drexel University

[2]Department of Neurobiology and Anatomy, Drexel University College of Medicine

ABSTRACT

The influence of neural activity on astrocytes and their reciprocal interactions with neurons has emerged as an important modulator of synapse function. Activity regulates gene expression in astrocytes, yet the molecular mechanisms by which such activity is translated into functional changes in gene expression have remained largely unknown. The molecular signaling pathway, Sonic hedgehog (Shh), mediates neuron-astrocyte communication and regulates the organization of cortical synapses. Here, we demonstrate that sensory experience stimulates SHH signaling in cortical astrocytes. Whisker stimulation and chemogenetic activation both increase SHH activity in deep layers of the somatosensory cortex, where neuron-astrocyte SHH signaling is predominantly found. Selective loss of SHH signaling in astrocytes occludes experience-dependent structural plasticity of synapses. We further demonstrate that sensory experience promotes expression of the synapse modifying molecules, Hevin and SPARC, in a SHH-dependent manner. Taken together, these data identify SHH signaling as an activity-dependent, neuronal derived cue that stimulates astrocyte interactions with synapses and promotes synaptic plasticity.

23 **INTRODUCTION**

24 Bidirectional communication between neurons and astrocytes plays an important role in modulating
25 synapse function. Astrocytes associate intimately with synapses, comprising the third partner in the
26 tripartite synapse, along with the pre and postsynaptic terminals[1]. They express a large complement of
27 receptors, transporters, and ion channels[2-4], enabling them to monitor and respond to neural activity[5-7]
28 and reciprocally regulate synapse function[8-13]. This is accomplished through Ca^{2+}-mediated
29 gliotransmission[14] as well as activity-dependent changes in astrocyte gene expression. These activity-
30 dependent transcriptional responses are as robust as many classes of neurons[10,15]. Notably, activity
31 also regulates expression of several genes associated with synapse formation and function[6,16,17],
32 suggesting influential roles for astrocytes in activity-dependent synaptic plasticity. The precise
33 molecular mechanism by which astrocytes translate neuronal activity into changes in gene expression
34 remain poorly defined.

35

36 The molecular signaling pathway, Sonic hedgehog (Shh) is emerging as an important mediator of
37 reciprocal interactions between neurons and astrocytes. During embryonic development, SHH exerts
38 considerable regulation over various gene expression programs in neural precursor cells and immature
39 neurons that drive a broad array of neurodevelopmental programs including proliferation, cell
40 specification, and axon pathfinding[18]. However, in the postnatal and adult brain, SHH mediates
41 communication between mature neurons and astrocytes[19]. Neurons in deep layers of the cortex
42 express SHH which acts directly on neighboring astrocytes, regulating SHH-dependent gene
43 expression programs[19-21]. Notably, genetic ablation of SHH signaling, selectively in astrocytes,
44 decreases expression of the glial-specific, inward rectifying K^+ channel, $K_{ir}4.1$, perturbing extracellular
45 K^+ homeostasis and increasing neuronal excitability[22]. Conversely, unrestrained SHH signaling
46 promotes synapse formation mediated by increased expression of synaptogenic cues[21]. These
47 observations point to SHH as a key mediator of neuron-astrocyte interactions that shape synapse

48 number and function. Further, non-canonical SHH signaling in neurons is required for establishing
49 cortico-cortical synapses[23], suggesting diverse and cell-type specific actions of SHH on synaptic
50 regulation. Here, we focus on SHH signaling in astrocytes, mediated by canonical transduction of the
51 pathway.
52
53 Transduction of SHH signaling is mediated by transcriptional activation of its effectors, the GLI family of
54 transcription factors, that regulate expression of SHH target genes[24]. Binding of SHH to its receptor,
55 Patched (*Ptch1*), relieves inhibition of the obligatory co-receptor, Smoothened (*Smo*), promoting
56 transcription of SHH target genes, including *Gli1*. High levels of SHH promote transcriptional activation
57 of *Gli1*, which acts as a reliable readout of pathway activation[25]. At baseline, transcriptional abundance
58 of *Gli1* in the cortex is low[21] and its expression is localized to astrocytes in layers 4 and 5, consistent
59 with the distribution of SHH-expressing neurons in layer V[19,23]. However, several components of the
60 pathway, including *Ptch1*, *Gli2,* and *Gli3*, show more widespread expression[21]. Whereas cells
61 expressing *Gli1* at baseline comprise 40-50% of astrocytes in layers 4 and 5[22], the vast majority of cells
62 in these layers express *Ptch1*, *Gli2* and *Gli3*, indicating that many more cells possess the machinery for
63 transduction of SHH signal[19]. This suggests activation of the pathway in individual cells is dynamically
64 regulated. What regulates SHH signaling is not known. High frequency stimulation of cultured
65 hippocampal neurons promotes SHH release that is sensitive to TTX treatment[26], suggesting that
66 neural activity regulates SHH signaling. Interestingly, SHH protein is localized in axons[27-30], where it is
67 associated with synaptic vesicles[31]. Whether physiological neural activity promotes SHH-mediated
68 interactions between neurons and astrocytes *in vivo,* and how these interactions influence synapses, is
69 not known.
70
71 To test this, we exposed juvenile mice to an enriched somatosensory environment to stimulate active
72 whisking. We show that both sensory and chemogenetic stimulation increase SHH signaling in cortical
73 astrocytes. Exposure to an enriched environment produced an increase in synapse number and a

74 concomitant increase in expression of Hevin and SPARC, matricellular proteins released by astrocytes
75 that modify synaptic structure and function. Structural plasticity, and experience-dependent
76 upregulation of Hevin and SPARC, are occluded in conditional knock out (CKO) mice in which *Smo*, the
77 obligatory SHH co-receptor, is selectively abolished in astrocytes, demonstrating a requirement for
78 SHH signaling in astrocyte modulation of synapses. Taken together, these findings establish novel,
79 activity-dependent modulation of SHH signaling as a molecular mechanism by which neurons recruit
80 astrocytes during times of heightened activity.
81

82 # RESULTS

83 *Neuronal activity stimulates Sonic hedgehog signaling in vivo*

84 To examine whether neural activity stimulates SHH signaling *in vivo*, we used a chemogenetic
85 approach to selectively excite cortical pyramidal neurons with the excitatory hM3DGq designer receptor
86 exclusively activated by designer drugs (DREADD) (**Figure 1A-B**). We injected AAV8-CamKIIα-
87 hM3DGq-mCherry virus[32] into the somatosensory cortex of *Gli1*$^{nlacZ/+}$ mice which express nuclear lacZ
88 at the *Gli1* locus[25]. Because *Gli1* is a canonical target of SHH signaling, and because SHH is required
89 for *Gli1* expression, transcriptional activation of *Gli1* acts as a reliable readout of SHH signaling[25,33].
90 After 14 days, we treated mice with medicated drinking water containing the designer drug Clozapine
91 N-Oxide (CNO) for seven days to chronically activate the receptor[34]. Transfected cells expressed *c-Fos*
92 **(Figure 1C)**, and CNO-treated mice showed a significant increase in the number of c-Fos-labeled cells
93 compared to virus-injected animals that were fed unmedicated drinking water, indicating successful
94 activation of neurons (**Figure 1D-E**). We observed a significant increase in the number of βGal+ cells
95 in the somatosensory cortex in the CNO-treated group compared to untreated controls (**Figure 1F-G**).
96 These cells colocalized with Sox9, a well-established marker for identifying astrocytes[35] (**Figure 1H**).
97 Taken together, these data demonstrate that neuronal excitation stimulates SHH signaling in astrocytes
98 *in vivo*.

99 *Sensory experience stimulates Sonic hedgehog signaling*

100 We next examined whether a more physiological stimulus can increase SHH signaling. To test this,
101 we placed *Gli1*$^{nlacZ/+}$ mice in an enriched sensory environment designed to stimulate active whisking.
102 Mice were weaned into large rat cages from which strings of beads were hung from the wire cage lid in
103 a manner requiring constant interaction[36] at postnatal day 21 (P21). Control mice were weaned into
104 similar rat cages with only standard nesting materials and no beads. Mice were housed in the enriched
105 environment (EE) or standard housing (SH) conditions for three weeks (**Figure 2A**). A significant
106 increase in the number of cells labeled with cFos was observed in the somatosensory cortex of mice
107 housed in EE compared to SH conditions (**Figure 2C**), confirming increased activity in this region. Mice
108 housed in EE showed a significant increase in the number of βGal-labeled cells compared to control
109 mice housed in SH conditions (**Figure 2B, D**), indicating an increase in SHH activity in response to
110 sensory experience. There was no difference in the number of βGal cells between sexes at baseline
111 and both males and females showed similar increases in βGal cell number after exposure to EE
112 (**Supplemental Figure 1**).
113
114 We next examined whether exposure to EE produces a generalized increase in SHH activity throughout
115 the cortex or whether activity of the pathway increased specifically in the somatosensory cortex, the
116 region targeted by the EE paradigm used here. We analyzed the visual cortex and found no difference
117 in either cFos or βGal labeling between EE and SH conditions (**Figure 2E-F**), indicating that SHH
118 signaling is selectively increased in circuits that are stimulated by activity. Colocalization with cell-type
119 specific markers including Sox9, CAII, and NeuN to identify astrocytes, oligodendrocytes, and neurons,
120 respectively, showed that 96% of βGal-labeled cells correspond to astrocytes in both SH and EE
121 (**Supplemental Figure 2**) consistent with our previous observation that astrocytes are the primary
122 targets of canonical SHH signaling in the adult brain[19]. βGal+ cells did not express Ki-67
123 (**Supplemental Figure 2**), ruling out the possibility that the observed increase in cell number is due to
124 proliferation. Because sensory activity stimulates SHH signaling, we next asked whether sensory

125 deprivation lowers activity of the pathway. To do this, we performed unilateral whisker trimming on P21
126 *Gli1*$^{nlacZ/+}$ mice for three weeks, starting at birth. We analyzed the deprived, contralateral hemisphere
127 and compared it to the intact, ipsilateral hemisphere. We observed significantly fewer βGal+ cells in the
128 deprived, compared to the intact, hemisphere (**Supplemental Figure 3**). Analysis of the auditory cortex
129 showed whisker trimming had no effect on SHH signaling in this region (**Supplemental Figure 3**).
130 Taken together, these data demonstrate that activation of distinct sensory circuits selectively stimulates
131 SHH signaling in cortical astrocytes in a circuit-specific manner.
132
133 To precisely identify cells that show increased SHH activity following experience, we combined the
134 direct reporter approach with a tamoxifen-dependent labeling strategy, enabling us to monitor
135 temporally distinct populations of cells experiencing SHH signaling. We crossed *Gli1*$^{nlacZ/+}$ mice with
136 *Gli1*$^{CreER/+}$;Ai14 mice carrying the Cre-dependent Ai14 reporter allele expressing tdTomato (tdTom)
137 (*Gli1*$^{nlacZ/CreER}$;Ai14), enabling identification of cells with SHH signaling at the start and conclusion of
138 sensory enrichment. Because *lacZ* expression is directly regulated by transcriptional activity of *Gli1*,
139 cells actively transducing SHH can be monitored by immunohistochemistry for βGal, the protein product
140 of the *lacZ* gene. In contrast, tamoxifen-dependent, Cre-mediated recombination produces permanent
141 expression of tdTom in cells, even after SHH activity is downregulated (**Figure 2G**). Thus, in
142 *Gli1*$^{nlacZ/CreER}$;Ai14 mice, *lacZ* expression reflects active SHH signaling whereas tamoxifen-dependent
143 Cre-mediated expression of tdTom reflects historical signaling. Although these mice are effectively *Gli1*
144 nulls, GLI1 is dispensable for SHH signaling due to redundant activator function of GLI2[25,37] and we did
145 not observe any gross anatomical or behavioral phenotypes, consistent with previous studies[25,38]. To
146 mark cells with SHH signaling at baseline, mice received tamoxifen before placing them in EE or SH
147 housing for three weeks (**Figure 2G**). We first examined the population of βGal+ cells and found a large
148 fraction of cells that were negative for tdTom (**Figure 2H, I**), indicating SHH activity in a population of
149 cells distinct from those marked at the start of the experiment. Notably, there was a significant increase
150 in single-labeled βGal cells after EE compared to SH (**Figure 2J**). Whereas 59% of βGal labeled cells

151 were single labeled in SH mice, this fraction increased to 76% in EE mice (**Figure 2J**) demonstrating
152 experience-dependent activation of the pathway in cells distinct from those at baseline. These cells
153 were found in layers 4 and 5 (**Figure 2H**), suggesting that experience-dependent SHH activity remains
154 localized to deep cortical layers, consistent with the localization of SHH-expressing neurons in layer
155 V[19,23]. We next examined the population of cells expressing tdTom. Cells expressing tdTom were
156 localized primarily in layers 4 and 5 and show a bushy morphology characteristic of protoplasmic
157 astrocytes, consistent with previous studies[19,22] (**Figure 2H-I**). In SH mice, a large proportion of
158 tdTom+ cells did not colabel with βGal (**Figure 2I, K**), indicating downregulation of pathway activity.
159 This fraction did not change after exposure to EE (**Figure 2K**). We also observed a third population of
160 cells, those co-expressing both tdTom and βGal, suggesting either persistent or recurrent SHH activity
161 in these cells (**Figure 2I, L**). This fraction was similar between SH and EE conditions (**Figure 2L**).
162 These data suggest that SHH activity in individual cells is highly dynamic and that over a three-week
163 period, individual cells are not likely to experience persistent SHH signaling.
164
165 *Sensory experience dynamically modulates Sonic hedgehog signaling*
166 We next examined whether the experience-induced increase in SHH activity reflects a long-term
167 change in SHH signaling. We first examined whether a much shorter time frame was sufficient to
168 increase SHH activity. We housed *Gli1*$^{nlacZ/+}$ mice in either SH or EE for two days starting at P21. Mice
169 housed in EE showed a significant increase in βGal+ cells compared to SH controls (**Figure 3A-B**),
170 suggesting that brief exposure to sensory enrichment is sufficient to stimulate SHH signaling. To
171 examine whether experience-dependent SHH signaling persists after removal of the stimulus, we
172 housed *Gli1*$^{nlacZ/+}$ mice in EE for 2 days, then housed them in SH conditions for 2 days and compared
173 *Gli1* activity with mice continuously housed in EE or SH conditions for 4 days. To rule out the possibility
174 that any observed differences in βGal number may reflect perdurance of the protein rather than
175 sustained SHH activity, we used single molecule fluorescent *in situ* hybridization (smFISH) by
176 RNAScope to more directly measure *Gli1* transcripts (**Figure 3C**). In mice continuously housed in EE,

177 we found an increase in cells expressing *Gli1* compared to SH control mice (**Figure 3C-D**). However,
178 in mice returned to SH after 2 days of EE, *Gli1* expression returned to baseline (**Figure 3C-D**).
179 Notably, individual cells expressing *Gli1* also showed an increase in the number of transcripts in the
180 nucleus after exposure to EE compared to SH-housed mice (**Figure 3C**). This suggests that neural
181 activity stimulates SHH signaling in new cells while those with baseline SHH signaling experience
182 further increases in activity of the pathway. The number of *Gli1*-expressing cells was selectively higher
183 in layers 4 and 5, while no significant changes were found in upper layers (**Figure 3D**), consistent with
184 the localization of SHH-expressing neurons. These data demonstrate that SHH signaling is highly
185 dynamic and responsive to changing experiences.
186
187 *Sensory experience does not increase the number of SHH-expressing neurons*
188 In the cortex, SHH is expressed predominantly in a subset of excitatory pyramidal neurons in layer V.
189 To determine whether sensory experience increases the number or distribution of *Shh*-expressing cells,
190 we housed $Shh^{CreER/+}$; Ai14 mice in EE or SH conditions and administered tamoxifen at the conclusion
191 of the experiment (**Figure 4A**). Labeled neurons were found primarily in layer V and we found no
192 difference in the number of *Shh*-expressing neurons between SH and EE (**Figure 4B-E**). Because
193 astrocytes in layer IV show high levels of SHH activity, we also examined the ventral posterior medial
194 nucleus of the thalamus (VPM) where thalamocortical neurons projecting to layer IV of the barrel cortex
195 reside[39]. We detected few, if any, labeled neurons in this region (**Figure 4D**) suggesting that SHH
196 signaling in cortical astrocytes is initiated by ligand released from local neurons. We also performed
197 chemogenetic activation of cortical neurons in $Shh^{CreER/+}$;Ai14 mice. We injected mice with AAV5-Syn-
198 hM3DGq-HA virus and began CNO treatment two weeks later. Animals received CNO or unmedicated
199 water for 10 days. To mark *Shh*-expressing cells, animals received tamoxifen over the last three days
200 of CNO treatment and were analyzed two weeks later (**Figure 4F**). In agreement with our
201 environmental stimulation, there was no difference in the number or distribution of *Shh*-expressing cells
202 between the CNO treated and control animals (**Figure 4G-J**). These data suggest that the increase in

203 astrocytic signaling reflects an increase in availability of the ligand, rather than an increase in the
204 number of neurons expressing *Shh*. This may arise from an increase in its release or from increased
205 diffusion in the extracellular space. This suggests that while transduction of SHH signaling in
206 astrocytes is dynamically modulated between individual cells, SHH ligand is derived from a defined
207 population of neurons.
208
209 *Experience-dependent structural plasticity requires Sonic hedgehog signaling*
210 Sensory experience promotes structural plasticity of cortical synapses[36]. To determine whether
211 experience-dependent SHH signaling in astrocytes promotes synaptic plasticity, we examined dendritic
212 spines of layer V cortical neurons. Excitatory synapses are localized predominantly on dendritic
213 spines[40], which demonstrate remarkable plasticity in response to sensory experience[36,41-44]. Selective
214 loss of SHH signaling in astrocytes leads to elevated spine density of layer V cortical neurons, arising
215 from an increase in spine stability[22], while unrestrained SHH activity in astrocytes promotes synapse
216 formation[21]. To determine whether SHH signaling plays a role in astrocyte modulation of experience-
217 dependent plasticity, we examined spine density in conditional knock out (CKO) mice lacking *Smo*
218 selectively in astrocytes. We used *Gfap-Cre*; *Smo*$^{fl/fl}$ mice (*Gfap Smo* CKO) in which *Smo* is deleted in
219 *Gfap*-expressing cells, effectively abolishing SHH signaling in all astrocytes beginning at birth[19,22].
220 These mice also carry a *Thy1*-GFPm allele which labels a subset of layer V pyramidal neurons[45],
221 enabling the visualization of individual dendrites and spines. *Gli1* expression measured by qPCR
222 showed a 90% reduction in *Gfap Smo* CKO mice compared to WT littermate controls lacking Cre,
223 confirming effective ablation of SHH activity (**Supplemental Figure 4**). We analyzed apical dendrites
224 of layer V pyramidal neurons in the barrel cortex, focusing on dendritic segments in layers 4 and 5
225 where high levels of SHH activity are found. WT (Cre-negative) mice housed in EE conditions showed
226 a significant increase in the density of protrusions compared to control SH mice (**Figure 5A,C**),
227 demonstrating that enriched sensory experience promotes synaptic plasticity, consistent with previous
228 studies[36,43]. We previously demonstrated that *Gfap Smo* CKO mice showed an elevated spine density

229 arising from deficits in developmental elimination of synapses[22]. Here, we find that sensory enrichment
230 did not produce any further increases in spine density (**Figure 5B,C**), consistent with a requirement for
231 astrocytic SHH signaling in structural plasticity. Alternatively, this may instead reflect a limit beyond
232 which no further spines can be added. SHH signaling acts on astrocyte progenitor cells in the perinatal
233 subventricular zone that generate cortical astrocytes[38]. Because recombination begins at P0 in cortical
234 astrocyte progenitors in this Gfap-Cre line[19], this impaired plasticity may reflect developmental
235 perturbation of cortical astrocyte development.
236
237 To more directly test whether SHH signaling in mature astrocytes is required for synaptic plasticity, we
238 generated *Gli1*$^{CreER/+}$; *Smo*$^{fl/fl}$; Ai14 mice (*Gli1 Smo* CKO) in which *Smo* is selectively deleted in
239 astrocytes expressing *Gli1* in a tamoxifen-dependent manner. This approach enabled greater temporal
240 and spatial control over *Smo* deletion. Tamoxifen administration at P14 or older limits *Smo* deletion to
241 postmitotic, *Gli1* expressing cells primarily in layers 4 and 5 (**Figure 5D**)[38]. *Gli1 Smo* CKO mice
242 received tamoxifen over three days between P18 – P20 and were housed in EE or SH at P21 for two
243 days. We measured *Gli1* expression by qPCR of cortical tissues and detected a 66% reduction in *Gli1*
244 transcripts in *Gli1 Smo* CKO mice compared to WT littermate controls that were Cre-negative,
245 confirming effective interruption of SHH signaling (**Supplemental Figure 4**). Analysis of dendritic
246 segments in deep layers showed no significant difference in spine density between SH and EE
247 conditions, indicating that experience-dependent structural plasticity is impaired in *Gli1 Smo* CKO
248 (**Figure 5E,F**). To determine whether plasticity is perturbed globally, we analyzed regions where SHH
249 activity in astrocytes is low or absent. Notably, analysis of dendritic segments in upper layers (layers II/
250 III) showed a significantly higher spine density in mice housed in EE compared to SH (**Figure 5G**),
251 suggesting that structural plasticity of these synapses is intact. We also analyzed apical dendrites of
252 pyramidal neurons in area CA1 of the hippocampus, which lack astrocytic SHH activity (**Figure 5H**).
253 Mice housed in EE also showed a significant increase in spine density compared to SH (**Figure 5I**),
254 further supporting the specificity of this mouse model. Taken together, these data demonstrate that

255 SHH signaling in astrocytes promotes structural plasticity induced by enriched sensory experience.
256 The observation that plasticity is impaired specifically in synapses found where astrocytic SHH activity
257 is high suggests that SHH-dependent astrocyte modulation of synaptic plasticity is mediated by local
258 interactions.
259
260 *Sonic hedgehog signaling upregulates expression of astrocyte-derived synapse-modifying cues*
261 In the developing neural tube, SHH regulates the expression of genes that drive morphogenesis and
262 cell type specification. In astrocytes, several lines of evidence demonstrate that SHH regulates genes
263 associated with synapse formation and function, including *Sparc, Kcnj10*, and *Gria1*[20-22].
264 The observation that structural plasticity is impaired in *Gli1 Smo* CKO mice suggests that SHH
265 regulates an astrocyte-derived synaptogenic cue. Hevin is a matricellular protein belonging to the
266 SPARC family of proteins that is expressed in astrocytes and promotes synapse formation[46-49]. To
267 examine whether experience-dependent SHH activity regulates *Hevin*, we examined its expression in
268 the cortex of *Gli1*$^{CreER/+}$;Ai14 mice. Analysis of Hevin immunostaining in the cortex shows an
269 enrichment in layers IV and V, where SHH activity is highest (**Figure 6A and Supplemental Figure**
270 **5A**). Single cell analysis of deep and upper layer astrocytes in *Gli1*$^{CreER/+}$;Ai14 mice revealed that
271 astrocytes in layers IV and V, identified by tdTom labeling, express higher levels of Hevin compared to
272 those in layer II/ III, identified by Sox9 (**Figure 6B-D**), suggesting that SHH signaling regulates its
273 expression. To test this, we measured *Hevin* from whole cortical lysates of *Gfap Smo* CKO mice by
274 qPCR and found a significant reduction in expression compared to WT controls (**Figure 6E**). *Hevin*
275 expression was not completely abolished in *Gfap Smo* CKO mice, suggesting that SHH signaling may
276 cooperate with additional mechanisms to regulate *Hevin*. We next examined secreted acidic cysteine
277 rich glycoprotein (SPARC), a structurally related protein to Hevin that is secreted by astrocytes and
278 which also acts to modify synapses *in vitro* and *in vivo*[49,50]. Expression of *Sparc* is upregulated in *Glast*
279 *Ptch1* CKO mice in which SHH signaling is elevated in astrocytes due to removal of PTCH-mediated
280 inhibition of SMO[21]. Similar to Hevin, SPARC expression was enriched in layers IV and V relative to

281 upper layer astrocytes in WT mice (**Figure 6F and Supplemental Figure 5B**) and single cell analysis
282 of individual cells confirmed this observation (**Figure 6G-I**). There was a significant reduction in *Sparc*
283 expression in *Gfap Smo* CKO mice compared to WT controls (**Figure 6J**), demonstrating a requirement
284 for SHH signaling, and extending the observations reported by Xie et al., 2022. Neither *Hevin* nor
285 *Sparc* expression were completely abolished in *Gfap Smo* CKO mice, indicating multiple regulatory
286 pathways for these genes. Indeed, although their expression is higher in deep layers of the cortex, their
287 expression is not absent in upper layers (**Figure 6A and F; Supplemental Figure 5**). Taken together,
288 these data show that *Hevin* and *Sparc* are enriched in deep layer astrocytes and further demonstrate a
289 requirement for SHH signaling in regulating their expression.
290
291 We next asked whether experience-dependent SHH activity promotes an increase in expression of
292 these synapse modifying cues. We performed immunostaining for Hevin and SPARC in *Gli1*$^{nlacZ/+}$ mice
293 and analyzed their expression selectively in βGal+ cells following EE or SH. Mice housed in EE
294 showed a pronounced increase in Hevin and SPARC compared to SH controls (**Figure 7A-F**),
295 demonstrating that enriched sensory experience promotes upregulation of these proteins. To
296 determine whether SHH signaling is required for the experience-dependent increase in these proteins,
297 we examined their expression in astrocytes in *Gfap Smo* CKO mice following two-day exposure to EE
298 or SH. In these mice, EE failed to increase expression of Hevin or SPARC (**Figure 7G-L**),
299 demonstrating a requirement for SHH signaling in experience-dependent upregulation of these genes.
300
301 Hevin and SPARC act, respectively, to modify synapses structurally and functionally. Whereas Hevin
302 promotes the formation of spines with a mushroom morphology[49], SPARC has been shown to increase
303 the number of GluA1 containing AMPA receptors at synapses[51]. We analyzed spine morphology,
304 classifying them into mushroom, thin, and filopodial morphologies and examined whether the proportion
305 of spines in each class change in response to experience and SHH signaling. Spine morphology is
306 associated with synapse size and strength[52,53]. In WT mice housed in EE, we observed an increase in

307 the proportion of spines with a mushroom morphology (**Figure 7N**), consistent with previous reports
308 demonstrating that activity promotes the enlargement of spines[54]. This was accompanied by a
309 concomitant reduction in the fraction of intermediate spines and filopodia (**Supplemental Figure 6B,**
310 **F**). In contrast, the proportion of mushroom spines was similar between EE and SH conditions in both
311 *Gfap Smo* CKO and *Gli1 Smo* CKO mice (**Figure 7O-P**) indicating that selective perturbation of SHH
312 signaling in astrocytes interferes with activity-dependent spine enlargement. These mice also showed
313 no difference in the fraction of spines with an intermediate or filopodia morphology between EE and SH
314 conditions (**Supplemental Figure 6C,G**). These data suggest that SHH signaling in astrocytes
315 promotes the activity-dependent enlargement of spines with intermediate or filopodia morphologies into
316 spines with a mushroom morphology. We next examined whether sensory experience increases GluA1
317 AMPA receptors in dendritic spines. Only a small fraction of spines contained GluA1 receptors and this
318 did not change following exposure to EE (**Figure 7R**). In *Gli1 Smo CKO* mice, the fraction of spines
319 with GluA1 was similar to that observed in WT mice and did not change following EE (**Supplemental**
320 **Figure 7**), arguing against a role for SHH signaling or SPARC in synaptic GluA1. Alternatively, it is
321 possible that the levels of SPARC induced by activity in this paradigm are insufficient to promote GluA1
322 AMPARs at the synapse. Only intermediate concentrations of SPARC were sufficient to increase
323 synaptic GluA1 AMPARs in culture[51]. Further experiments are necessary to determine whether a
324 stronger stimulus or more prolonged exposure to sensory enrichment promotes a greater increase in
325 SPARC expression and concomitant GluA1 AMPARs. Nevertheless, taken together, these data show
326 that enriched sensory experience upregulates expression of Hevin and SPARC in a SHH-dependent
327 manner.
328

329 ## DISCUSSION

330 In this study, we demonstrate that neural activity stimulates SHH signaling between neurons and
331 astrocytes. Activity of the pathway is highly dynamic and responsive to both an increase and decrease

332 in neural activity, key features for effective translation of neural activity into functional molecular
333 programs. Selective perturbation of SHH signaling in astrocytes occludes an experience-dependent
334 increase in spine number, suggesting that activity of the pathway is required for structural synaptic
335 plasticity in cortical neurons. Neural activity also promotes expression of Hevin and SPARC,
336 matricellular proteins known to modify synapses. Notably, upregulation of Hevin and SPARC in
337 response to activity requires intact SHH signaling. Taken together, these data demonstrate that neural
338 activity stimulates SHH signaling, initiating bidirectional communication between neurons and
339 astrocytes that promotes synaptic plasticity.
340
341 A large body of evidence now shows that astrocytes respond directly to neural activity. Glutamate
342 elicits Ca^{2+} signaling[55,56] that promotes the release of gliotransmitters, including glutamate, ATP and D-
343 serine[57]. Neural activity also regulates expression of astrocyte genes, including those that regulate
344 synapse formation and function[58]. Yet the molecular mechanisms by which astrocytes translate neural
345 activity into changes in gene expression have not been identified. Here we show that neural activity
346 modulates SHH signaling between neurons and astrocytes. Neural activity generated by either
347 chemogenetic or environmental stimulation increased SHH signaling and conversely, sensory
348 deprivation or removal of the stimulus downregulated the pathway. Notably, activity-dependent SHH
349 signaling was selectively increased in appropriate circuits as stimulation of the somatosensory cortex
350 did not increase activity of the pathway in the visual cortex. While the number of astrocytes transducing
351 SHH increases following EE, the number of neurons expressing *Shh* remains consistent between EE
352 and SH conditions. This suggests that SHH signaling is initiated by a defined population of neurons
353 that signals to neighboring astrocytes in a dynamically regulated manner such that increased neural
354 activity recruits additional astrocytes. In this way, SHH signaling cooperates with glutamatergic
355 signaling to recruit astrocytes during times of heightened neuronal activity, promoting astrocyte
356 interactions with synapses. These experiments were performed on mice at P21, corresponding to the
357 end of critical period plasticity for the somatosensory cortex[59], suggesting that SHH signaling mediates

358 astrocyte modulation of mature, relatively established circuits. Several lines of evidence point to a role
359 for SHH in regulating synapses. Genetic activation of the pathway selectively in astrocytes increases
360 cortical synapse density that is mediated through upregulation of synapse-modifying genes[21].
361 Consistent with this, our data show that the synaptogenic cues, Hevin and SPARC, are regulated by
362 SHH signaling. Interestingly, selective loss of SHH signaling in astrocytes from birth also increases
363 synapse number. However this phenotype arises due to perturbation in developmental elimination of
364 cortical synapses, leading to elevated synapse number that persists into adulthood[22]. Collectively,
365 these observations demonstrate two essential features of astrocytic SHH signaling. First, SHH acts on
366 astrocytes in mature circuits, as well as during the initial establishment of circuits in postnatal
367 development, regulating gene expression programs that promote astrocyte modulation of synapses.
368 Second, the mechanisms by which astrocytic SHH signaling modulates synapses vary with respect to
369 circuit maturity. In established circuits, SHH signaling promotes synaptic plasticity through the
370 regulation of astrocyte-derived synapse modifying cues. During postnatal development, as nascent
371 neural circuits are being formed, SHH signaling acts to ensure appropriate organization and function of
372 synapses. Thus, SHH is a versatile cue that regulates astrocyte modulation of synapses.
373
374 Astrocyte modification of synapses is mediated by a diverse repertoire of molecular cues, including the
375 release and secretion of matricellular and cell adhesion molecules[60,61]. Constitutive activation of SHH
376 signaling in cortical astrocytes increases SPARC expression[21], suggesting SHH is sufficient for its
377 upregulation. Here, we extend this finding and report that selective interruption of pathway activity in
378 astrocytes significantly decreases SPARC expression, demonstrating a requirement for SHH signaling
379 in regulating SPARC. We further demonstrate that Hevin, a structurally related protein with
380 synaptogenic function, is also SHH-dependent. Immunohistochemical labeling, together with genetic
381 marking of *Gli1*-expressing astrocytes, shows that these proteins are enriched in cells with SHH
382 activity. It should be noted that although *Gli1*-expressing astrocytes in deep layers show higher levels
383 of SPARC and Hevin, upper layer astrocytes also express these proteins, suggesting that their

384 expression is regulated by additional mechanisms that remain to be discovered. Our data further show
385 that sensory experience upregulates SPARC and Hevin expression in deep layer astrocytes and that
386 this requires intact SHH signaling. Hevin promotes the structural formation of synapses through its
387 interactions with neurexin and neuroligin and also promotes spine maturation[49,62]. Our data show that
388 both spine density and the proportion of spines with a mushroom morphology increase in a SHH-
389 dependent manner following sensory experience. Taken together, these observations are consistent
390 with the idea that experience-dependent structural plasticity is mediated by upregulation of Hevin in a
391 SHH-dependent manner. In contrast to Hevin, the actions of SPARC on synapses are less well
392 understood. SPARC has been shown to both antagonize and promote synapses[48,51]. Our data
393 showing that synapse density increases following sensory experience, despite an increase in SPARC
394 expression, would seem to be in conflict with reports that SPARC antagonizes the synaptogenic actions
395 of Hevin. An intriguing possibility is that Hevin and SPARC are differentially upregulated at specific
396 synapses, enabling local regulation by specific perisynaptic astrocyte processes. shRNA knockdown of
397 SPARC in astrocytes selectively reduces cortico-cortical VGlut1-labeled synapses, but not
398 thalamocortical VGlut2-labeled synapses in deep layers[21]. Both the Hevin and SPARC antibodies used
399 in this study were raised in the same species, precluding a direct test of this possibility, however future
400 studies including EM approaches are necessary to fully elucidate the role of SPARC in SHH-dependent
401 astrocyte modulation of synapses.
402
403 Here, we focus on SHH activity in the somatosensory cortex. However, SHH signaling is found
404 throughout multiple cortical regions, including in the auditory and visual cortex, as well as in the frontal
405 cortex[19]. This suggests that SHH signaling is broadly available to various circuits as a molecular
406 mechanism by which neurons can recruit astrocytes during periods of heightened activity to support
407 synaptic function and plasticity. Though found in multiple cortical regions, in the hippocampus,
408 astrocytic SHH signaling is largely absent[19,22] and instead is found predominantly in adult neural stem
409 cells[63], where its activity is required for their maintenance[64,65]. This suggests that astrocytic SHH

410 signaling, though widespread throughout the forebrain, regulates discrete circuits. Notably, differential
411 activity of the pathway is also found within a given region. Genetic deletion of SHH signaling,
412 selectively in layers IV and V, does not perturb structural plasticity in layer II/III, suggesting that
413 astrocyte modulation of synapses is mediated by distinct mechanisms, even within a defined circuit.
414
415 Although active SHH signaling is found predominantly in deep cortical layers, several components of
416 the pathway, including *Gli2*, *Gli3,* and *Ptch1* are found in upper layer astrocytes[19], suggesting these
417 cells fail to receive sufficient ligand to initiate pathway activity. This suggests that promoting SHH
418 availability to upper layer astrocytes would promote similar effects on synapses. In support of this,
419 ectopic expression of *Shh* in upper layer neurons promotes expression of SHH target genes, including
420 *Sparc* and *Kcnj10*[21]. The precise mechanism restricting SHH to deep layers is not known. In
421 development, the SHH gradient is established by interactions with extracellular matrix (ECM) proteins,
422 including heparin sulfate proteoglycans (HSPGs)[66]. In *Drosophila*, the movement of Hedgehog (Hh)
423 across cells is regulated by Dally and Dally-like, two glypicans that colocalize with Hh and act to restrict
424 its movement[67]. Recent work in vertebrate cells suggests that loss of glypican 5 (*gpc5*) broadens the
425 spread of SHH[66], suggesting that glypican-mediated regulation of SHH movement is conserved. The
426 related glypicans, glypican 4 and 6, are expressed by astrocytes and regulate AMPA receptor
427 composition at the synapse[68] and more recently, *gpc5* has been shown to regulate GluA2 at the
428 synapse and promote synapse stabilization[69]. This suggests that SHH signaling and glypicans work
429 cooperatively in astrocyte modulation of synaptic function.
430
431 Precisely how SHH is released from neurons is poorly understood. Several lines of evidence point to
432 axonal trafficking and release[70,71], consistent with activity-dependent release. Studies in cell culture
433 and by EM demonstrate that SHH is localized with synaptic vesicles[31] and is released by high
434 frequency stimulation[26]. Although cells with *Gli1* activity are found most abundantly in layers IV and V
435 of the cortex, we found few *Shh*-expressing neurons in the thalamus. Instead, SHH is found

436 predominantly in layer V pyramidal neurons, suggesting that SHH activity in the cortex is derived from
437 local neuronal sources, rather than long distance projections. This may arise from recurrent collateral
438 innervation by layer IV and V neurons[39]. SHH is also found in extracellular vesicles[72,73], specialized
439 vesicles derived from endosomes carrying diverse cargoes, including proteins, lipids and RNA
440 molecules, that mediate cell-cell communication. Exosome release is stimulated by neuronal activity[74].
441 The localization of *Gli1*-expressing cells in deep cortical layers, adjacent to *Shh*-expressing soma, is
442 consistent with an exosomal source of SHH, though release of SHH from synaptic vesicles from
443 recurrent collaterals cannot be ruled out. Interestingly, our genetic labeling experiments demonstrated
444 that activity did not increase the number of neurons expressing SHH. This suggests that activity
445 increases the number of synaptic vesicles or exosomes releasing ligand, enabling greater availability in
446 the extracellular space to reach more cells. Further work with SHH fusion proteins to identify its
447 localization within specific cellular compartments could shed light on the precise mechanism by which
448 neurons release SHH.
449

450 **Acknowledgements**

451 We gratefully acknowledge Dr. Corey Harwell and Dr. Lucas Cheadle for thoughtful comments on this
452 manuscript and throughout the project. The authors would also like to acknowledge Pooja Sakthivel for
453 technical support on this project, as well as all members of the Garcia lab.
454

455 **Author Contributions**

456 Conceptualization, A.D.L., M.F., A.D.R.G.; Investigation, A.D.L., M.F., R.K., G.Z.; Writing A.D.L. and
457 A.D.R.G.; Review and editing, A.D.L. and A.D.R.G.; Funding acquisition, A.D.R.G.; Supervision
458 A.D.R.G.
459

460 **Declaration of Interests**

461 The authors declare no competing interests.

462 **Key Resources Table**

REAGENT or RESOURCE	SOURCE	IDENTIFIER
Antibodies		
Polyclonal Goat anti SPARC	R&D Systems	AF942
Polyclonal Goat anti SPARC-like 1 (SPARCL1/ Hevin)	R&D Systems	AF2836
Polyclonal Chicken anti β-Gal	Abcam	AB9361
Polyclonal Rabbit anti β-Gal	Invitrogen	A-11132
Polyclonal Rabbit anti c-Fos	Cell Signaling	2250S
Polyclonal Rabbit anti Sox9	Novus	NVP1-85551
Polyclonal Rabbit anti NeuN	Novus	NBP2-10491
Polyclonal Sheep anti CAII	Serotec	AHP206
Polyclonal Rat anti HA	Sigma/ Roche	11867423001
Polyclonal Rabbit anti GluA1	Millipore Sigma	AB1504
Polyclonal Chicken anti GFP	Invitrogen	A10262
Mouse Strains		
Gfap-Cre (line 73.12)[75]	The Jackson Laboratory;	Stock no. 12886
Gli1$^{CreER/+63}$	The Jackson Laboratory;	Stock no. 7913
Gli1$^{nlacZ/+25}$		
Shh$^{CreER/+76}$		
Ai14 (B6.Cg-Gt(ROSA)26Sor$^{tm14(CAG-tdTomato)Hze}$/J)[77]	The Jackson Laboratory;	Stock no. 7914
Smo$^{fl/fl78}$	The Jackson Laboratory;	Stock no. 4526
Thy1-GFPm[45]	The Jackson Laboratory;	Stock no. 7788

Oligonucleotides		
Hevin CACTCCGAGTAGTCCCTCCA (forward) AAACTGTGAGTGGTGAGCGA (reverse)	Invitrogen	
Sparc TAGCTGCTCGGAGGGGAATGT (forward) TCACCATCCGCATGTTCCCAC (reverse)	Invitrogen	
Gli1 AACATGGCGTCTCAGGGAAG (reverse) GACGGAGGTCTCTTTGTCCG (forward)	Invitrogen	
Gapdh CATGGCCTACATGGCCTCCA (forward) TGGGATAGGGCCTCTCTTGCT (reverse)	Invitrogen	
Viral Constructs		
AAV8-CaMKIIa-hM3D(Gq)-mCherry	Addgene	50476-AAV8
AAV5-hSyn-hM3D(Gq)-HA	Addgene	121539-AAV5

Software		
PRISM	GraphPad	
ImageJ	Fiji	
CFX Manager	Bio-Rad	

463

464 # METHODS

465 *Animals*

466 All experiments were approved by Drexel University's Institutional Animal Care and Use Committee and
467 were conducted according to approved protocols. Transgenic mouse lines are listed in the key
468 resources table, used on the C57BL/6 background. Postnatal (P) day 18 – 90 mice were used for this
469 study. Mice of both sexes were included in each experiment.

470

471 *Enriched experience housing*

472 P21 littermates were weaned into either enriched environment (EE) or standard housing (SH) cages for
473 two days or three weeks. Large rat cages were used. The EE cage contained strings of beads hung
474 from wire lids, positioned densely throughout the cage, with the density and spacing altered every 3
475 days to promote novelty. The SH cage contained only standard hub and nesting materials. A minimum
476 of 7 mice was used for each cage. Data from each analysis was collected over 2-5separate
477 experiments from separate litters.

478

479 *Whisker trimming*

480 Whisker trimming procedure was conducted on P21 mice. Mice were anesthetized with isoflurane in an
481 induction chamber (3%) and then placed under dissecting scope with continuous isoflurane inhalation
482 (1.5%). Micro scissors were used to trim whiskers on the right side, as close to the skin as possible.
483 Whiskers were trimmed every 3 days, for the duration of 3 weeks.

484
485 *Tamoxifen administration*

486 Tamoxifen (Sigma) was dissolved in corn oil at a 20 mg/ml concentration at 37°C. Mice received 3
487 doses of 250mg/kg tamoxifen by oral gavage over 3 days and tissues were analyzed 2 days or 2-3
488 weeks after the last dose. For enriched experience and chemogenetic stimulation, tamoxifen was
489 administered during the last days of stimulation.

490

491 *Virus injection*

492 All AAV injections were conducted on adult mice at P60 or older. Immediately prior to surgery, mice
493 received a subcutaneous injection of carprofen (Rimadyl, 6.8 mg/kg), and a follow up injection given the
494 day after surgery. Mice were anesthetized with isoflurane in an induction chamber (3%) and then
495 placed in a stereotaxic apparatus (Stoelting) with continuous isoflurane inhalation (1.5%). The scalp
496 was opened and a small area of the skull was removed near injection site. Stereotaxic coordinates for
497 somatosensory cortex injection were AP -1.5 mm, ML -2.5 mm, DV -0.5 mm.

498

499 Viruses were stored in aliquots at -80°C and kept on ice until injection. Virus titers were ≥ 3×10^{12} vg/mL
500 for AAV8-CaMKIIa-hM3D(Gq)-mCherry and ≥ 7×10^{12} vg/mL for AAV5-hSyn-hM3D(Gq)-HA. Virus was
501 front-filled into a glass syringe (Hamilton). Injection volume was 1000 nL, delivered at 200 nL/ min
502 controlled by microinjector (WPI). After injection, mice were allowed to recover for 2 weeks before
503 administration of CNO (Tocris). CNO was dissolved in drinking water, aimed to deliver a dosage of 1mg
504 CNO per kg mouse over 1 week. Control mice received water only.

505
506
507 *Collection of animal tissue*

508 Animals used in experiments were each assigned a unique 4-5 digit ID in order to blind researchers.
509 Mice were deeply anesthetized by intraperitoneal injection of ketamine/ xylazine/ acepromazine,
510 transcardially injected with 100 units heparin and perfused with ice-cold PBS followed by 4%

511 paraformaldehyde (PFA; Sigma-Aldrich). Brains were dissected and fixed for at least 4 hours in PFA at
512 4ºC then transferred to 30% sucrose at 4ºC for at least 48 hours. Brains were cryosectioned (Leica
513 CM3050s) and collected in 40 µm sections. Sections were stored in 0.1M Tris-buffered saline (TBS)
514 with 0.05% sodium azide at 4ºC. Immunohistochemistry was performed with primary antibodies listed in
515 the resources table below. Sections were washed three times with 0.1M TBS at room temperature (10
516 minutes/wash) then blocked in 10% Normal Serum with 0.5% Triton-X (Sigma-Aldrich) for one hour at
517 room temperature. Sections were then incubated with primary antibody in 0.5% Triton-X at 4ºC
518 overnight.
519
520 *Immunohistochemistry*
521 For fluorescent immunohistochemistry, sections were rinsed for three times the following day in 0.1M
522 TBS and incubated in AlexaFluor-conjugated secondary antibodies with 10% Normal Serum in 0.1M
523 TBS at room temperature for two hours. Sections were then rinsed in 0.1M TBS and incubated in DAPI
524 (Life Technologies) for 15 minutes. Sections were rinsed again in 0.1M TBS, mounted on microscope
525 slides (Fisherbrand), and coverslipped using ProLong Gold Antifade Mounting Medium (Invitrogen
526 #P10144) and Fisherfinest Premium Cover Glass. For brightfield immunohistochemistry, sections were
527 rinsed as previously described but were incubated with biotinylated secondary antibodies against the
528 primary species (Vector Laboratories) for one hour. Sections were transferred to Avidin-Biotin Complex
529 solution (Vector) for one hour and visualized using 3,3'-diaminobenzadine (DAB Peroxidase Substrate
530 Kit, Vector). Sections were then mounted onto slides as described, dehydrated through increasing
531 concentrations of EtOH, and cover slipped with DPX mounting medium (Fisher).
532
533 *Fluorescent In situ hybridization (RNAscope)*
534 All fluorescent in-situ hybridization (FISH) experiments were performed on brain tissue fixed with 4%
535 paraformaldehyde and processed using cryosectioning at 14 µm and directly slide mounted, with one
536 brain section per slide. The assay was carried out using the "fixed frozen sample preparation and

537 treatment" and the RNAscope Multiplex Fluorescent v2 Assay using the manufacturer's instructions.
538 The original protocol can be found here on the ACDBio website: https://acdbio.com/documents/product-
539 documents.
540
541 Confocal z-stack images were acquired at 63x for blinded analysis in ImageJ (FIJI). Cells with at least 4
542 puncta were identified as positive for *Gli1* expression. The number of *Gli1*+ cells were divided by the
543 total number of DAPI cells within the z-stack, and then normalized to SH condition. For each animal,
544 each layer, at least 2 z-stacks were analyzed for a minimum of 100 DAPI cells.
545
546 *Stereological quantification*
547 The number of cells in each area of the cortex was estimated using a modified optical fractionator and
548 stereological image analysis software (Stereo Investigator, MBF Bioscience) with upright microscope
549 (Zeiss) with a computer-driven stage. The cortical area of interest (somatosensory, motor or visual
550 cortex) was outlined at a low magnification, using anatomical landmarks as described in Paxinos and
551 Franklin's The Mouse Brain in Stereotaxic Coordinates 4th Ed. For somatosensory cortex, sections
552 from A-P Bregma 1.33mm to -2.15mm were analyzed. For visual cortex, sections from A-P Bregma -
553 2.27mm to -4.59mm were analyzed. A target cell count of 150 and target coefficient of error (m=1) of <
554 0.1 was used to define number of sections counted, scan grid, and counting frame size. Counting
555 frames were randomly selected by the image analysis software and cells were counted at the 40x
556 objective with a DIC optic filter. Only cells with a clearly labeled cell body were counted.
557
558 *Fluorescent intensity analysis*
559 Immunofluorescent slides were imaged using Leica DMI 4000B microscope equipped with TCS SPE
560 confocal system. Regions of interest were identified with 10x dry objective and confocal z-stacks were
561 acquired with 40x or 63x oil objectives. To analyze protein abundance in a single astrocyte, a 20 μm x
562 20 μm region of interest is drawn in ImageJ around an astrocyte identified by fluorescent signal of

563 either tdTomato, βGal or Sox9 staining as astrocyte marker. This region of interest only contains one
564 astrocyte of interest and not contain signal from other cells. The mean fluorescent intensity and
565 histogram from one z-plane is collected. At least 25 cells were sampled per animal, dispersed
566 throughout multiple sites encompassing the somatosensory cortex. The mean fluorescent intensities of
567 the cells were averaged to produce the fluorescent intensity value for one animal, represented in the
568 graph as one data point.
569
570 *Dendritic spine analysis*
571 Analysis of spine density was performed in a blinded study design. WT controls were derived from Cre-
572 negative littermates. For analysis in the cortex, apical dendrites of layer V pyramidal neurons located in
573 layers II/III, IV and V were imaged. For analysis in the hippocampus, apical dendrites from CA1
574 pyramidal neurons were imaged. Confocal z-stacks were collected with 63x oil objective, at 0.35 μm
575 steps. Spine density was determined by first tracing the dendritic segment in ImageJ and obtaining the
576 length. Analyzed segments range from 75 – 125 μm. Protrusions were classified into mushroom,
577 intermediate or filopodial morphologies. Protrusions exhibiting a bright, bulbous head with a large head-
578 to-stalk ratio were classified as mushroom. Thinner protrusions with a dimmer, smaller or no head were
579 classified as intermediate. Dim, thin and elongated protrusions that lack any head were classified as
580 filopodia. For GluA1 colocalization analysis in dendritic spines, 63x z-stack images were analyzed.
581 Only spine heads colocalizing with a clearly defined GluA1 puncta were categorized as positive for
582 GluA1 (such as in Figure 7). The number of GluA1 positive protrusions were divided by the total
583 number of protrusions on the segment to obtain the fraction of GluA1 positive protrusions.
584
585 *Quantitative reverse transcriptase – polymerase chain reaction (qRT-PCR)*
586 Mice were deeply anesthetized by isoflurane before rapid decapitation. Cortices were dissected into
587 TRIzol reagent (Thermo-Fisher, Waltham, MA) and RNA was extracted according to TRIzol's standard
588 protocol. RNA was reverse transcribed to cDNA using the High-Capacity cDNA Reverse Transcription

589 Kit (Thermo-Fisher). qPCR was performed with the CFX96 Touch Real-Time PCR Detection System
590 (Bio-Rad) using PowerUp SYBR Green Master Mix (Thermo-Fisher). Primers were designed using
591 NCBI Primer-BLAST (see resources table). Samples were run in triplicate. Data were analyzed using
592 the CFX Manager Software (Bio-Rad), using the ΔΔCt method. Gapdh was used as the reference
593 gene, itself having no difference of expression between sample groups.
594
595 *Quantification and statistical analysis*
596 Statistical analysis and data visualization were performed using Prism (GraphPad). Welch's t-tests,
597 one-way ANOVA with multiple comparisons, two-way ANOVA with multiple comparisons, pair-wise t-
598 tests were used with reported p-values. In all graphs, data points represent individual animals.
599

600 # FIGURE LEGENDS

601 **Figure 1. Neuronal activity stimulates SHH signaling.**
602 **(A)** Schematic depicting experimental approach. *Gli1*$^{nlacZ/+}$ mice were injected with AAV8-CamKIIα-
603 hM3DGq-mCherry in the somatosensory cortex. Two weeks later, mice were fed CNO-medicated or
604 unmedicated drinking water for 7 days before analysis. **(B)** Transfected region can be visualized with
605 mCherry. SSCtx, somatosensory cortex. Scale bar, 250 μm. **(C)** mCherry (magenta, left panel) and c-
606 Fos (green, middle panel) in transfected region. Arrows point to cells co-expressing mCherry and c-
607 Fos. Scale bar, 25 μm. **(D, G)** Brightfield immunohistochemistry for c-Fos (D) and βGal (G) in the
608 somatosensory cortex. Scale bar, 25 μm. **(E, H)** Stereological quantification of c-Fos (E) and βGal (H)
609 in the transfected region shows increased neural activity and increased SHH signaling in mice that
610 received CNO compared to water-fed controls. **(F)** Immunofluorescent staining for Sox9 (magenta, left
611 panel) and βGal (green, middle panel) in transfected region. Arrows point to βGal cells co-labeled with
612 Sox9. Scale bar, 25 μm. Data points represent individual animals; bars show mean ± SEM; Welch's t-
613 test.

614 **Figure 2. Enriched experience stimulates SHH signaling.**

615 **(A)** Experimental timeline. *Gli1*$^{nlacZ/+}$ mice were weaned into standard housing (SH) or enriched
616 experience (EE) cages at P21 and analyzed at P42. **(B)** Representative brightfield
617 immunohistochemistry for βGal in the somatosensory cortex. Scale bar, 50 μm. **(C-F)** Stereological
618 quantification of cells expressing the immediate-early gene *c-Fos* (C, E) or βGal (D, F) in the
619 somatosensory (C, D) or visual (E, F) reveals increased activity and SHH signaling in the
620 somatosensory cortex, but not visual cortex. **(G)** Schematic depicting genetic strategy to label cells with
621 temporally distinct SHH signaling (left panel) and timeline of experiment (right panel). In *Gli1*$^{nlacZ/+}$ mice,
622 βGal expression labels cells with active SHH signaling. In *Gli1*^{CreER};Ai14 mice, Cre-mediated
623 recombination promotes permanent expression of tdTom. In *Gli1*$^{CreER/nlacZ}$;Ai14 mice, tdTom expression
624 identifies cells with SHH signaling at baseline (t_0) and βGal expression identifies SHH signaling in cells
625 at the end of the experiment (t_1). Double labeled cells identify cells with persistent SHH signaling
626 throughout the experiment. **(H-I)** Low power (H) and high power (I) images showing tdTom expression
627 (magenta, left panel) and immunostaining for β-Gal (green, middle panel; merged image, right panel) in
628 the cortex of mice housed in EE as described in (G). Scale bar, 250 μm. (I) Individual cells show those
629 with upregulation (blue arrowhead), downregulation (open arrowhead) and persistent (white arrow)
630 SHH activity. Scale bar, 50 μm. **(J-L)** The fraction of βGal-labeled cells that are single labeled (J),
631 tdTom-labeled cells that are single labeled (K), and all cells that are double labeled (L) in SH or EE.
632 Data points represent individual animals; bars show mean ± SEM; Welch's t-test.
633

634 **Figure 3. SHH signaling responds rapidly to sensory activation and is not persistent.**

635 **(A)** Brightfield immunohistochemistry for β-Gal in the somatosensory cortex of *Gli1*$^{nlacZ/+}$ mice housed in
636 SH (upper panel) or EE (lower panel) for 2 days. Scale bar, 50 μm. **(B)** Stereological quantification of β-
637 Gal shows increased SHH activity in the somatosensory cortex after 2 days of EE. **(C)** Representative
638 images of fluorescent *in situ* hybridization for *Gli1* mRNA in deep layers of the cortex from SH, EE,
639 EE+SH housing conditions. Dotted line outlines individual DAPI nuclei with *Gli1* mRNA. Note the

640 increase in *Gli1* transcripts in EE compared to SH. Scale bar, 10 µm. **(D)** Fraction of DAPI nuclei
641 positive for *Gli1* mRNA in Layers II/ III, IV and V of the cortex from mice housed in SH or EE for 4 days
642 or EE for 2 days followed by SH for 2 days (EE+SH). In each layer, at least 50 cells analyzed per
643 animal. Data points represent individual animals; data represent mean ± SEM; Welch's t-test (B) and
644 one-way ANOVA with multiple comparisons (D). Only p values <0.05 are shown. *p < 0.05, **p < 0.01,
645 n.s. not significant.
646
647 **Figure 4. Sensory experience does not increase the number of Shh-expressing neurons.**
648 **(A)** Schematic depicting experimental approach. P21 *Shh*$^{CreER/+}$; Ai14 mice were weaned into SH or EE
649 cages at P21 and received 3 doses of tamoxifen from P39 - P41. Tissues were analyzed two weeks
650 after the last tamoxifen dose. **(B-D)** Low power image showing tdTom labeled cells (magenta) in
651 *Shh*$^{CreER/+}$; Ai14 mice. Labeled cells are found predominantly in layer V. Insets show individual cells
652 with neuronal morphology in the cortex (C) and no labeled cells in the ventral posterior medial (VPM)
653 nucleus of the thalamus (D). Counterstained with DAPI (blue). Scale bar, 25 µm. **(E)** The number of
654 *Shh* neurons in the cortex in SH and EE mice. **(F)** *Shh*$^{CreER/+}$; Ai14 mice were injected with AAV5-hSyn-
655 hM3DGq-HA targeting the somatosensory cortex. After 2 weeks, mice were fed CNO-medicated or
656 unmedicated water for 10 days, receiving 3 doses of tamoxifen during the last 3 days. Tissues were
657 analyzed seven days later. dpi, days post injection. **(G-I)** Immunolabeling for HA (green) shows the
658 transduced region overlapping with tdTom labeled (magenta) cells in the cortex. Inset shown in (H).
659 Individual cell shown at high power in (I). Scale bar, 25 µm. **(J)** The number of *Shh* neurons in the
660 cortex between water control versus CNO. Data points represent individual animals; bars show mean ±
661 SEM; Welch's t-tests.
662
663 **Figure 5. Experience-dependent structural plasticity requires SHH signaling.**
664 **(A-B)** Representative dendritic segments in deep layers of WT (A) and *Gfap Smo* CKO (B) mice
665 housed in SH or EE. Scale bar, 5 µm. **(C)** Spine density of dendritic segments in deep layers of WT and

666 *Gfap Smo* CKO mice housed in SH or EE. **(D)** tdTom (magenta) labeled astrocytes and GFP (white)
667 labeled neurons in the cortex of WT (C) and *Gli1 Smo* CKO (D) mice. Scale bar, 100 µm. **(E)** Dendritic
668 segments from *Gli1 Smo* CKO mice housed in SH or EE. **(F)** Spine density of dendritic segments in
669 deep layers is shown. **(G)** Spine density of upper layer dendritic segments from WT (left) and *Gli1 Smo*
670 CKO (right) mice. **(H)** tdTom (magenta) and GFP (white) labeled cells in area CA1 of the hippocampus
671 from WT and *Gli1 Smo* CKO mice, counterstained with DAPI (blue). Area CA1 contains few tdTom
672 labeled cells reflecting the absence of Shh activity in hippocampal astrocytes. Scale bar, 50 µm. **(I)**
673 Spine density from apical dendrites of CA1 neurons in *Gli1 Smo* CKO mice housed in SH or EE. Data
674 points represent individual animals, bars show mean ± SEM, $n \geq 3 - 5$ dendritic segments analyzed per
675 animal. Statistical testing performed by two-way ANOVA or Welch's t-test. s.o., stratum oriens; s.r.,
676 stratum radiatum.
677
678 **Figure 6. SHH signaling regulates expression of astrocyte-derived synapse-modifying cues**
679 **Hevin and SPARC.**
680 **(A, F)** Low power images of the cortex from *Gli1*$^{CreER/+}$*;* Ai14 showing tdTom cells (magenta, left panels)
681 localized primarily in deep layers and immunofluorescent staining for Hevin (A, gray) and SPARC (F,
682 gray) (middle panels) shows that Hevin and SPARC are enriched in deep layer astrocytes. Merged
683 images in right panels. (**B-C, G-H**) Individual cells from upper layer (Layer II/ III) labeled with Sox9
684 (green, B, G) and deep layers (Layers IV & V) labeled with tdTom (magenta, C, H). Scale bar, 10 µm.
685 **(D, I)** Single cell analysis of fluorescence intensity of Hevin (D) and SPARC (I) immunostaining in upper
686 and deep layer astrocytes. *n=3* animals, 50 cells analyzed per animal. **(E, J)** qPCR for *Hevin* (E) or
687 *Sparc* (J) expression in WT vs *Gfap Smo* CKO mice. *Hevin* and *Sparc* expression are significantly
688 lower in CKO mice compared to WT controls. *n=13* WT mice, *n=8 Gfap Smo* CKO. Data points
689 represent individual animals; bars show mean ± SEM; Welch's t-tests.
690

691 **Figure 7. Experience-dependent Hevin and SPARC are SHH-dependent.**

692 **(A-B, D-E)** Immunofluorescent staining for βGal (green, left panels, A, B, D, E) and Hevin (gray, middle
693 panels, A, B) or SPARC (middle panels, D, E) in *Gli1*$^{nlacZ/+}$ mice housed in SH vs EE. Merged images in
694 right panels. Scale bar, 10 μm. **(C, F)** Single cell analysis of Hevin (C) or SPARC (F) fluorescent
695 intensity in βGal-labeled cells. *n=5-6* mice in SH, *n=7* mice in EE, 50 cells analyzed per animal. **(G-H,**
696 **J-K)** Immunostaining for Sox9 (green, left panels, G, H, J, K) and Hevin (gray, middle panels, G, H) or
697 SPARC (gray, middle panels, J, K) in *Gfap Smo* CKO mice housed in SH vs EE. Merged images in
698 right panels. Scale bar, 10 μm. **(I, L)** Single cell analysis of Hevin (I) or SPARC (L) fluorescent
699 intensity in Sox9-labeled astrocytes. *n=3-5* mice in SH, *n=4-6* mice in EE, 25 cells analyzed per animal.
700 Scale bar, 10 μm. **(M)** Representative examples of protrusions categorized as mushroom spines
701 (arrows). Scale bar, 5 μm. **(N-P)** Fraction of mushroom spines from WT (N), *Gfap Smo* CKO (O) and
702 *Gli1 Smo* CKO (P) mice after SH vs EE. *n=2-6* mice from SH, *n=4-6* mice from EE, at least 300 spines
703 from 3 dendritic segments analyzed per animal. **(Q)** Immunostaining for GluA1 (magenta) in dendritic
704 spines. Arrow points to spine colocalizing with GluA1 puncta. Scale bar, 5 μm. **(R-T)** The fraction of
705 GluA1+ protrusions in WT (R), *Gfap Smo* CKO (S) and *Gli1 Smo* CKO (T) mice after SH or EE. *n=2-6*
706 mice in SH, *n=3-5* mice in EE, at least 200 spines analyzed per animal. Data points represent
707 individual animals; bars show mean ± SEM; Welch's t-tests.
708

709 **Figure S1: There is no difference in SHH activity between males and females. Related to Figure**
710 **2.**

711 **(A)** Stereological quantification of βGal cells in the somatosensory cortex at baseline from P42 *Gli1*$^{nlacZ/+}$
712 mice between males and females; *n=4* mice. **(B-C)** Stereological quantification of βGal cells in males
713 (B) and females (C) housed in SH and EE; *n=3-8* mice in SH, *n=6-10* mice in EE. Data pooled from 2
714 day and 21 day experiments. Data points represent individual animals; bars show mean ± SEM;
715 Welch's t-tests.
716

717 **Figure S2: Enriched experience stimulates SHH activity in astrocytes. Related to Figure 2.**

718 **(A-D)** Immunofluorescence for βGal (green), and Sox9 (A), NeuN (B), CAII (C) or Ki67 (D; magenta) in

719 the cortex of *Gli1*$^{nlacZ/+}$ mice. Counterstained with DAPI (blue). Merged images shown in right panels.

720 **(E)** The fraction of βGal-labeled cells colocalizing with Sox9 does not change between SH and EE. *n=4*

721 mice in SH, *n=5* mice in EE, 100-400 βGal cells analyzed per animal. Scale bar, 10 μm; data points

722 represent individual animals; bars show mean ± SEM; Welch's t-test.

723

724 **Figure S3: Whisker deprivation reduces SHH activity.**

725 **(A-B)** Stereological quantification of βGal cells from the ipsilateral (intact) and contralateral (deprived)

726 barrel (A) and auditory (B) cortex after 3 weeks of unilateral whisker trimming. *n=3* mice, data points

727 represent individual animals, bars show mean ± SEM; Paired t-tests.

728

729 **Figure S4: SHH activity is effectively disrupted in Smo CKO mice without altering spine density**

730 **at baseline. Related to Figure 5.**

731 **(A-B)** qPCR for *Gli1* expression in WT and *Gfap Smo* CKO (A) and *Gli1 Smo* CKO (B) mice. *n=4-6*

732 mice. **(C)** Representative dendritic segments from WT versus *Gli1 Smo* CKO at baseline. Scale bar, 5

733 μm. **(D)** Protrusion density between WT versus *Gli1 Smo* CKO at baseline. *n=2* WT mice, *n=3 Gli1*

734 *Smo* CKO mice, 3 dendritic segments analyzed per animal. Data points represent individual animals;

735 bars show mean ± SEM; Welch's t-tests (A, D), and one-way ANOVA with multiple comparisons (B).

736

737 **Figure S5: Hevin and SPARC are enriched in deep layers of the cortex where SHH signaling is**

738 **active. Related to Figure 6.**

739 **(A-B)** Fluorescence intensity measurements of Hevin (A) and SPARC (B) across cortical layers. *n=5-7*

740 animals, 2 sections analyzed per animal. Data points represent individual animals; bars show mean ±

741 SEM; one-way ANOVA with multiple comparisons. Only p values < 0.05 are reported.

742

743 **Figure S6: Experience-dependent maturation of dendritic spines requires SHH activity. Related**
744 **to Figure 7.**
745 **(A)** Apical dendrites from layer V neurons, arrows point to intermediate spines. Scale bar, 5 µm.
746 **(B-D)** Fraction of intermediate spines in WT (B), *Gfap Smo* CKO (C) and *Gli1 Smo* CKO (D) mice after
747 exposure to SH or EE housing. *n=2-6* mice for SH, *n=4-6* mice for EE. **(E)** Apical dendrites from layer
748 V neurons, arrow points to filopodia. Scale bar, 5 µm. **(F-H)** Fraction of filopodia in WT (F), *Gfap Smo*
749 CKO (G) and *Gli1 Smo* CKO (H) mice after exposure to SH or EE housing. *n=2-6* mice for SH, *n=4-6*
750 mice for EE. Data points represent individual animals; bars show mean ± SEM; Welch's t-tests.
751

752 # REFERENCES

753 1 Perea, G., Navarrete, M. & Araque, A. Tripartite synapses: astrocytes process and control
754 synaptic information. *Trends Neurosci* **32**, 421-431 (2009).
755 https://doi.org:10.1016/j.tins.2009.05.001

756 2 Ahmadpour, N. *et al.* Cortical astrocyte N-methyl-D-aspartate receptors influence whisker barrel
757 activity and sensory discrimination in mice. *Nat Commun* **15**, 1571 (2024).
758 https://doi.org:10.1038/s41467-024-45989-3

759 3 Liu, J., Feng, X., Wang, Y., Xia, X. & Zheng, J. C. Astrocytes: GABAceptive and GABAergic
760 Cells in the Brain. *Front Cell Neurosci* **16**, 892497 (2022).
761 https://doi.org:10.3389/fncel.2022.892497

762 4 Shelton, M. K. & McCarthy, K. D. Mature hippocampal astrocytes exhibit functional metabotropic
763 and ionotropic glutamate receptors in situ. *Glia* **26**, 1-11 (1999).
764 https://doi.org:10.1002/(sici)1098-1136(199903)26:1<1::aid-glia1>3.0.co;2-z

765 5 Armbruster, M. *et al.* Neuronal activity drives pathway-specific depolarization of peripheral
766 astrocyte processes. *Nature Neuroscience* **25**, 607-616 (2022). https://doi.org:10.1038/s41593-
767 022-01049-x

768 6 Farhy-Tselnicker, I. *et al.* Activity-dependent modulation of synapse-regulating genes in
769 astrocytes. *Elife* **10** (2021). https://doi.org:10.7554/eLife.70514

770 7 Hasel, P. *et al.* Neurons and neuronal activity control gene expression in astrocytes to regulate
771 their development and metabolism. *Nature Communications* **8**, 15132 (2017).
772 https://doi.org:10.1038/ncomms15132

773 8 Araque, A., Parpura, V., Sanzgiri, R. P. & Haydon, P. G. Tripartite synapses: glia, the
774 unacknowledged partner. *Trends in Neurosciences* **22**, 208-215 (1999).
775 https://doi.org:https://doi.org/10.1016/S0166-2236(98)01349-6

776 9 Halassa, M. M., Fellin, T. & Haydon, P. G. The tripartite synapse: roles for gliotransmission in
777 health and disease. *Trends in Molecular Medicine* **13**, 54-63 (2007).
778 https://doi.org:https://doi.org/10.1016/j.molmed.2006.12.005

779 10 Hrvatin, S. *et al.* Single-cell analysis of experience-dependent transcriptomic states in the
780 mouse visual cortex. *Nature Neuroscience* **21**, 120-129 (2018). https://doi.org:10.1038/s41593-
781 017-0029-5

782 11 Jourdain, P. *et al.* Glutamate exocytosis from astrocytes controls synaptic strength. *Nat*
783 *Neurosci* **10**, 331-339 (2007). https://doi.org:10.1038/nn1849

784 12 Sapkota, D. *et al.* Activity-dependent translation dynamically alters the proteome of the
785 perisynaptic astrocyte process. *Cell Rep* **41**, 111474 (2022).
786 https://doi.org:10.1016/j.celrep.2022.111474

787 13 Wang, F. *et al.* Photolysis of caged Ca2+ but not receptor-mediated Ca2+ signaling triggers
788 astrocytic glutamate release. *J Neurosci* **33**, 17404-17412 (2013).
789 https://doi.org:10.1523/jneurosci.2178-13.2013

790 14 Stobart, J. L. *et al.* Cortical Circuit Activity Evokes Rapid Astrocyte Calcium Signals on a Similar
791 Timescale to Neurons. *Neuron* **98**, 726-735.e724 (2018).
792 https://doi.org:https://doi.org/10.1016/j.neuron.2018.03.050

793 15 Hasel, P. *et al.* Neurons and neuronal activity control gene expression in astrocytes to regulate
794 their development and metabolism. *Nature Communications* **8**, 1-17 (2017).
795 https://doi.org:10.1038/ncomms15132

796 16 Genoud, C. *et al.* Plasticity of astrocytic coverage and glutamate transporter expression in adult
797 mouse cortex. *PLoS Biol* **4**, e343 (2006). https://doi.org:10.1371/journal.pbio.0040343

798 17 Allen, N. J. & Eroglu, C. Cell Biology of Astrocyte-Synapse Interactions. *Neuron* **96**, 697-708
799 (2017). https://doi.org:10.1016/j.neuron.2017.09.056

800 18 Zuñiga, N. R. & Stoeckli, E. T. Sonic Hedgehog—'Jack-of-All-Trades' in Neural Circuit
801 Formation. *Journal of Developmental Biology* **5** (2017).

802 19 Garcia, A. D. R., Petrova, R., Eng, L. & Joyner, A. L. Sonic Hedgehog Regulates Discrete
803 Populations of Astrocytes in the Adult Mouse Forebrain. *The Journal of neuroscience : the*
804 *official journal of the Society for Neuroscience* **30**, 13597-13608 (2010).
805 https://doi.org:10.1523/JNEUROSCI.0830-10.2010

806 20 Farmer, W. T. *et al.* Neurons diversify astrocytes in the adult brain through sonic hedgehog
807 signaling. *Science* **351**, 849-854 (2016). https://doi.org:10.1126/science.aab3103

808 21 Xie, Y. *et al.* Astrocyte-neuron crosstalk through Hedgehog signaling mediates cortical synapse
809 development. *Cell Reports* **38**, 110416 (2022).
810 https://doi.org:https://doi.org/10.1016/j.celrep.2022.110416

811 22 Hill, S. A. *et al.* Sonic hedgehog signaling in astrocytes mediates cell type-specific synaptic
812 organization. *eLife* **8**, e45545 (2019). https://doi.org:10.7554/eLife.45545

813 23 Harwell, Corey C. *et al.* Sonic Hedgehog Expression in Corticofugal Projection Neurons Directs
814 Cortical Microcircuit Formation. *Neuron* **73**, 1116-1126 (2012).
815 https://doi.org:https://doi.org/10.1016/j.neuron.2012.02.009

816 24 Briscoe, J. & Therond, P. P. The mechanisms of Hedgehog signalling and its roles in
817 development and disease. *Nat Rev Mol Cell Biol* **14**, 416-429 (2013).
818 https://doi.org:10.1038/nrm3598

819 25 Bai, C. B., Auerbach, W., Lee, J. S., Stephen, D. & Joyner, A. L. Gli2, but not Gli1, is required
820 for initial Shh signaling and ectopic activation of the Shh pathway. *Development* **129**, 4753-4761
821 (2002). https://doi.org:10.1242/dev.129.20.4753

822 26 Su, Y., Yuan, Y., Feng, S., Ma, S. & Wang, Y. High frequency stimulation induces sonic
823 hedgehog release from hippocampal neurons. *Sci Rep* **7**, 43865 (2017).
824 https://doi.org:10.1038/srep43865

825 27 Charytoniuk, D. *et al.* Sonic Hedgehog signalling in the developing and adult brain. *J Physiol*
826 *Paris* **96**, 9-16 (2002). https://doi.org:10.1016/s0928-4257(01)00075-4

827 28 Peng, J. *et al.* Sonic Hedgehog Is a Remotely Produced Cue that Controls Axon Guidance
828 Trans-axonally at a Midline Choice Point. *Neuron* **97**, 326-340 e324 (2018).
829 https://doi.org:10.1016/j.neuron.2017.12.028

830 29 Traiffort, E. *et al.* Discrete localizations of hedgehog signalling components in the developing
831 and adult rat nervous system. *Eur J Neurosci* **11**, 3199-3214 (1999).
832 https://doi.org:10.1046/j.1460-9568.1999.00777.x

833 30 Traiffort, E., Charytoniuk, D. A., Faure, H. & Ruat, M. Regional distribution of Sonic Hedgehog,
834 patched, and smoothened mRNA in the adult rat brain. *J Neurochem* **70**, 1327-1330 (1998).
835 https://doi.org:10.1046/j.1471-4159.1998.70031327.x

31 Beug, S. T., Parks, R. J., McBride, H. M. & Wallace, V. A. Processing-dependent trafficking of Sonic hedgehog to the regulated secretory pathway in neurons. *Molecular and Cellular Neuroscience* **46**, 583-596 (2011). https://doi.org:https://doi.org/10.1016/j.mcn.2010.12.009

32 Alexander, G. M. *et al.* Remote Control of Neuronal Activity in Transgenic Mice Expressing Evolved G Protein-Coupled Receptors. *Neuron* **63**, 27-39 (2009). https://doi.org:https://doi.org/10.1016/j.neuron.2009.06.014

33 Hui, C.-c. & Angers, S. Gli Proteins in Development and Disease. *Annual Review of Cell and Developmental Biology* **27**, 513-537 (2011). https://doi.org:10.1146/annurev-cellbio-092910-154048

34 Armbruster, B. N., Li, X., Pausch, M. H., Herlitze, S. & Roth, B. L. Evolving the lock to fit the key to create a family of G protein-coupled receptors potently activated by an inert ligand. *Proceedings of the National Academy of Sciences* **104**, 5163-5168 (2007). https://doi.org:10.1073/pnas.0700293104

35 Sun, W. *et al.* SOX9 Is an Astrocyte-Specific Nuclear Marker in the Adult Brain Outside the Neurogenic Regions. *The Journal of neuroscience : the official journal of the Society for Neuroscience* **37**, 4493 - 4507 (2017). https://doi.org:10.1523/jneurosci.3199-16.2017

36 Yang, G., Pan, F. & Gan, W.-B. Stably maintained dendritic spines are associated with lifelong memories. *Nature* **462**, 920-924 (2009). https://doi.org:10.1038/nature08577

37 Niewiadomski, P. *et al.* Gli Proteins: Regulation in Development and Cancer. *Cells* **8** (2019). https://doi.org:10.3390/cells8020147

38 Gingrich, E. C., Case, K. & Garcia, A. D. R. A subpopulation of astrocyte progenitors defined by Sonic hedgehog signaling. *Neural Development* **17**, 2 (2022). https://doi.org:10.1186/s13064-021-00158-w

39 Staiger, J. F. & Petersen, C. C. H. Neuronal Circuits in Barrel Cortex for Whisker Sensory Perception. *Physiological Reviews* **101**, 353-415 (2020). https://doi.org:10.1152/physrev.00019.2019

40 Nimchinsky, E. A., Sabatini, B. L. & Svoboda, K. Structure and function of dendritic spines. *Annual review of physiology* **64**, 313-353 (2002).

41 Chen, C.-C., Bajnath, A. & Brumberg, J. C. The Impact of Development and Sensory Deprivation on Dendritic Protrusions in the Mouse Barrel Cortex. *Cerebral Cortex* **25**, 1638-1653 (2015). https://doi.org:10.1093/cercor/bht415

42 Jung, C. K. E. & Herms, J. Structural Dynamics of Dendritic Spines are Influenced by an Environmental Enrichment: An In Vivo Imaging Study. *Cerebral Cortex* **24**, 377-384 (2014). https://doi.org:10.1093/cercor/bhs317

43 Landers, M. S., Knott, G. W., Lipp, H. P., Poletaeva, I. & Welker, E. Synapse formation in adult barrel cortex following naturalistic environmental enrichment. *Neuroscience* **199**, 143-152 (2011). https://doi.org:https://doi.org/10.1016/j.neuroscience.2011.10.040

44 Zuo, Y., Yang, G., Kwon, E. & Gan, W.-B. Long-term sensory deprivation prevents dendritic spine loss in primary somatosensory cortex. *Nature* **436**, 261-265 (2005). https://doi.org:10.1038/nature03715

45 Feng, G. *et al.* Imaging Neuronal Subsets in Transgenic Mice Expressing Multiple Spectral Variants of GFP. *Neuron* **28**, 41-51 (2000). https://doi.org:https://doi.org/10.1016/S0896-6273(00)00084-2

879 46 Bradshaw, A. D. Diverse biological functions of the SPARC family of proteins. *The International*
880 *Journal of Biochemistry & Cell Biology* **44**, 480-488 (2012).
881 https://doi.org:https://doi.org/10.1016/j.biocel.2011.12.021

882 47 Gan, K. J. & Südhof, T. C. SPARCL1 Promotes Excitatory But Not Inhibitory Synapse Formation
883 and Function Independent of Neurexins and Neuroligins. *J Neurosci* **40**, 8088-8102 (2020).
884 https://doi.org:10.1523/jneurosci.0454-20.2020

885 48 Kucukdereli, H. *et al.* Control of excitatory CNS synaptogenesis by astrocyte-secreted proteins
886 Hevin and SPARC. *Proc Natl Acad Sci U S A* **108**, E440-449 (2011).
887 https://doi.org:10.1073/pnas.1104977108

888 49 Risher, W. C. *et al.* Astrocytes refine cortical connectivity at dendritic spines. *eLife* **3**, e04047
889 (2014). https://doi.org:10.7554/eLife.04047

890 50 Albrecht, D. *et al.* SPARC prevents maturation of cholinergic presynaptic terminals. *Molecular*
891 *and Cellular Neuroscience* **49**, 364-374 (2012).
892 https://doi.org:https://doi.org/10.1016/j.mcn.2012.01.005

893 51 Jones, E. V., Bernardinelli, Y., Zarruk, J. G., Chierzi, S. & Murai, K. K. SPARC and GluA1-
894 Containing AMPA Receptors Promote Neuronal Health Following CNS Injury. *Frontiers in*
895 *Cellular Neuroscience* **12** (2018).

896 52 Arellano, J., Benavides-Piccione, R., DeFelipe, J. & Yuste, R. Ultrastructure of dendritic spines:
897 correlation between synaptic and spine morphologies. *Frontiers in Neuroscience* **1** (2007).

898 53 Holtmaat, A. & Svoboda, K. Experience-dependent structural synaptic plasticity in the
899 mammalian brain. *Nature Reviews Neuroscience* **10**, 647-658 (2009).
900 https://doi.org:10.1038/nrn2699

901 54 Matsuzaki, M., Honkura, N., Ellis-Davies, G. C. R. & Kasai, H. Structural basis of long-term
902 potentiation in single dendritic spines. *Nature* **429**, 761-766 (2004).
903 https://doi.org:10.1038/nature02617

904 55 Cornell-Bell, A. H., Finkbeiner, S. M., Cooper, M. S. & Smith, S. J. Glutamate induces calcium
905 waves in cultured astrocytes: long-range glial signaling. *Science* **247**, 470-473 (1990).
906 https://doi.org:10.1126/science.1967852

907 56 Porter, J. T. & McCarthy, K. D. Hippocampal astrocytes in situ respond to glutamate released
908 from synaptic terminals. *J Neurosci* **16**, 5073-5081 (1996). https://doi.org:10.1523/jneurosci.16-
909 16-05073.1996

910 57 Panatier, A. *et al.* Astrocytes are endogenous regulators of basal transmission at central
911 synapses. *Cell* **146**, 785-798 (2011). https://doi.org:10.1016/j.cell.2011.07.022

912 58 Sardar, D. *et al.* Induction of astrocytic Slc22a3 regulates sensory processing through histone
913 serotonylation. *Science* **380**, eade0027 https://doi.org:10.1126/science.ade0027

914 59 Pedrosa, L. R. R., Coimbra, G. d. S., Corrêa, M. G., Dias, I. A. & Bahia, C. P. Time Window of
915 the Critical Period for Neuroplasticity in S1, V1, and A1 Sensory Areas of Small Rodents: A
916 Systematic Review. *Frontiers in Neuroanatomy* **16** (2022).
917 https://doi.org:10.3389/fnana.2022.763245

918 60 Dallérac, G., Zapata, J. & Rouach, N. Versatile control of synaptic circuits by astrocytes: where,
919 when and how? *Nat Rev Neurosci* **19**, 729-743 (2018). https://doi.org:10.1038/s41583-018-
920 0080-6

921 61 Shan, L., Zhang, T., Fan, K., Cai, W. & Liu, H. Astrocyte-Neuron Signaling in Synaptogenesis.
922 *Frontiers in Cell and Developmental Biology* **9** (2021). https://doi.org:10.3389/fcell.2021.680301

923 62 Singh, S. K. *et al.* Astrocytes Assemble Thalamocortical Synapses by Bridging NRX1α and NL1
924 via Hevin. *Cell* **164**, 183-196 (2016). https://doi.org:10.1016/j.cell.2015.11.034

925 63 Ahn, S. & Joyner, A. L. In vivo analysis of quiescent adult neural stem cells responding to Sonic
926 hedgehog. *Nature* **437**, 894-897 (2005). https://doi.org:10.1038/nature03994

927 64 Balordi, F. & Fishell, G. Hedgehog signaling in the subventricular zone is required for both the
928 maintenance of stem cells and the migration of newborn neurons. *J Neurosci* **27**, 5936-5947
929 (2007). https://doi.org:10.1523/JNEUROSCI.1040-07.2007

930 65 Petrova, R., Garcia, A. D. & Joyner, A. L. Titration of GLI3 repressor activity by sonic hedgehog
931 signaling is critical for maintaining multiple adult neural stem cell and astrocyte functions. *J*
932 *Neurosci* **33**, 17490-17505 (2013). https://doi.org:10.1523/JNEUROSCI.2042-13.2013

933 66 Guo, W. & Roelink, H. Loss of the Heparan Sulfate Proteoglycan Glypican5 Facilitates Long-
934 Range Sonic Hedgehog Signaling. *Stem Cells* **37**, 899-909 (2019).
935 https://doi.org:10.1002/stem.3018

936 67 Han, C., Belenkaya, T. Y., Wang, B. & Lin, X. Drosophila glypicans control the cell-to-cell
937 movement of Hedgehog by a dynamin-independent process. *Development* **131**, 601-611
938 (2004). https://doi.org:10.1242/dev.00958

939 68 Allen, N. J. *et al.* Astrocyte glypicans 4 and 6 promote formation of excitatory synapses via
940 GluA1 AMPA receptors. *Nature* **486**, 410-414 (2012). https://doi.org:10.1038/nature11059

941 69 Bosworth, A. P. *et al.* Astrocyte glypican 5 regulates synapse maturation and stabilization.
942 *bioRxiv*, 2023.2003.2002.529949 (2023). https://doi.org:10.1101/2023.03.02.529949

943 70 Traiffort, E., Moya, K. L., Faure, H., Hässig, R. & Ruat, M. High expression and anterograde
944 axonal transport of aminoterminal sonic hedgehog in the adult hamster brain. *European Journal*
945 *of Neuroscience* **14**, 839-850 (2001).

946 71 Wallace, V. A. & Raff, M. C. A role for Sonic hedgehog in axon-to-astrocyte signalling in the
947 rodent optic nerve. *Development* **126**, 2901-2909 (1999).
948 https://doi.org:10.1242/dev.126.13.2901

949 72 Coulter, M. E. *et al.* The ESCRT-III Protein CHMP1A Mediates Secretion of Sonic Hedgehog on
950 a Distinctive Subtype of Extracellular Vesicles. *Cell Reports* **24**, 973-986.e978 (2018).
951 https://doi.org:https://doi.org/10.1016/j.celrep.2018.06.100

952 73 Vyas, N. *et al.* Vertebrate Hedgehog is secreted on two types of extracellular vesicles with
953 different signaling properties. *Sci Rep* **4**, 7357 (2014). https://doi.org:10.1038/srep07357

954 74 Sharma, P., Schiapparelli, L. & Cline, H. T. Exosomes function in cell-cell communication during
955 brain circuit development. *Curr Opin Neurobiol* **23**, 997-1004 (2013).
956 https://doi.org:10.1016/j.conb.2013.08.005

957 75 Garcia, A. D., Doan, N. B., Imura, T., Bush, T. G. & Sofroniew, M. V. GFAP-expressing
958 progenitors are the principal source of constitutive neurogenesis in adult mouse forebrain. *Nat*
959 *Neurosci* **7**, 1233-1241 (2004). https://doi.org:10.1038/nn1340

960 76 Harfe, B. D. *et al.* Evidence for an Expansion-Based Temporal Shh Gradient in Specifying
961 Vertebrate Digit Identities. *Cell* **118**, 517-528 (2004).
962 https://doi.org:https://doi.org/10.1016/j.cell.2004.07.024

963 77 Madisen, L. *et al.* A robust and high-throughput Cre reporting and characterization system for
964 the whole mouse brain. *Nature Publishing Group* **13**, 133-140 (2009).
965 https://doi.org:10.1038/nn.2467

966 78 Long, F., Zhang, X. M., Karp, S., Yang, Y. & McMahon, A. P. Genetic manipulation of hedgehog
967 signaling in the endochondral skeleton reveals a direct role in the regulation of chondrocyte
968 proliferation. *Development* **128**, 5099-5108 (2001). https://doi.org:10.1242/dev.128.24.5099

969

970

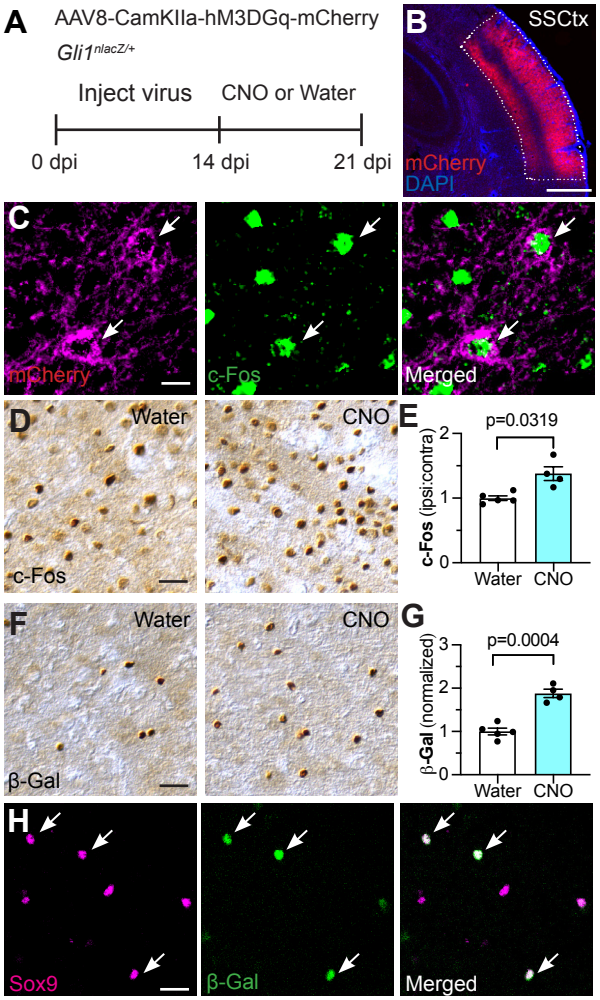

Figure 1. Neuronal activity stimulates SHH signaling. **(A)** Schematic depicting experimental approach. *Gli1*$^{nlacZ/+}$ mice were injected with AAV8-CamKIIα-hM3DGq-mCherry in the somatosensory cortex. Two weeks later, mice were fed CNO-medicated or unmedicated drinking water for 7 days before analysis. **(B)** Transfected region can be visualized with mCherry. SSCtx, somatosensory cortex. Scale bar, 250 µm. **(C)** mCherry (magenta, left panel) and c-Fos (green, middle panel) in transfected region. Arrows point to cells co-expressing mCherry and c-Fos. Scale bar, 25 µm. **(D, G)** Brightfield immunohistochemistry for c-Fos (D) and βGal (G) in the somatosensory cortex. Scale bar, 25 µm. **(E, H)** Stereological quantification of c-Fos (E) and βGal (H) in the transfected region shows increased neural activity and increased SHH signaling in mice that received CNO compared to water-fed controls. **(F)** Immunofluorescent staining for Sox9 (magenta, left panel) and βGal (green, middle panel) in transfected region. Arrows point to βGal cells co-labeled with Sox9. Scale bar, 25 µm. Data points represent individual animals; bars show mean ± SEM; Welch's t-test.

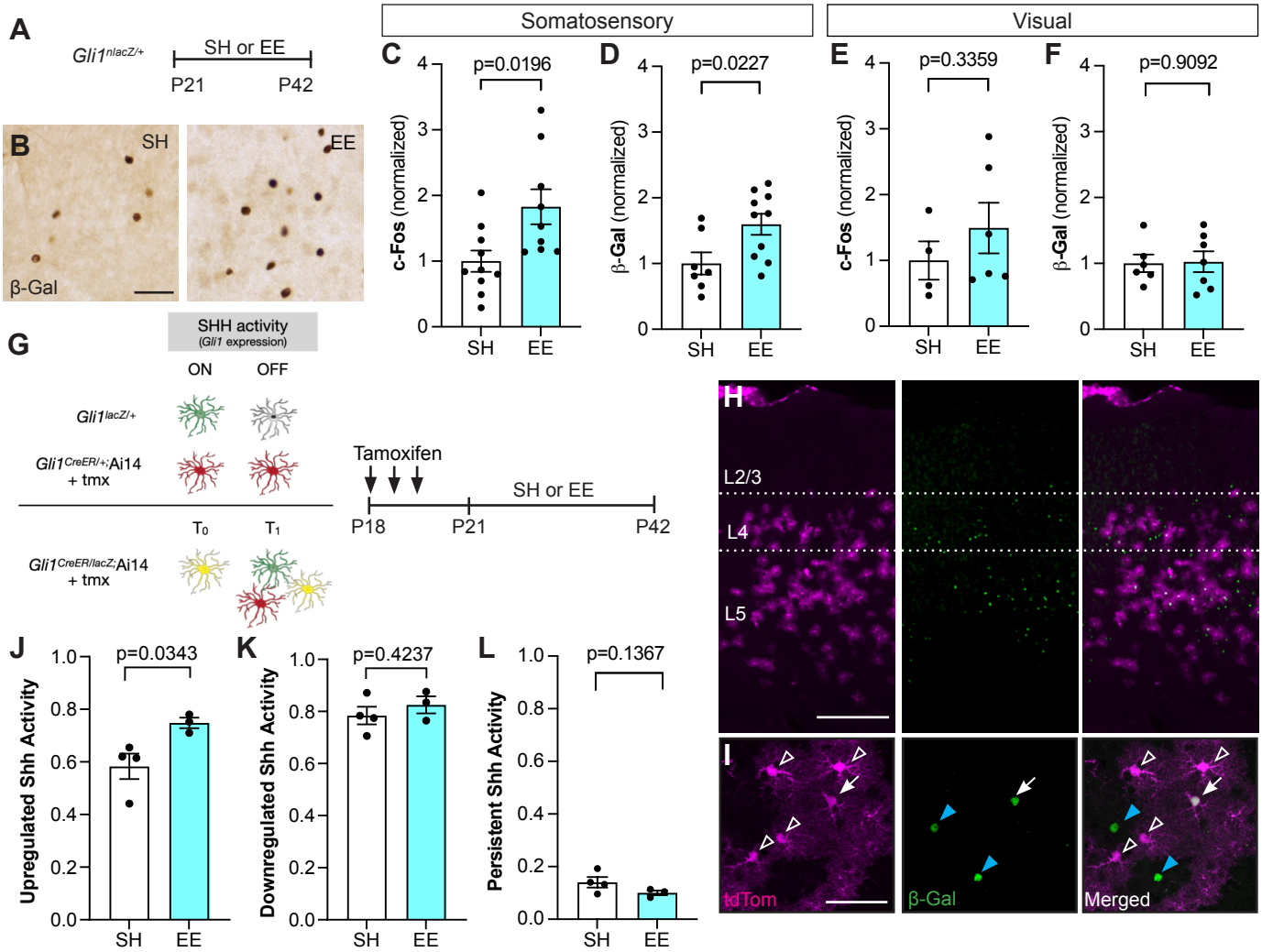

Figure 2. Enriched experience stimulates SHH signaling.
(A) Experimental timeline. *Gli1*$^{nlacZ/+}$ mice were weaned into standard housing (SH) or enriched experience (EE) cages at P21 and analyzed at P42. **(B)** Representative brightfield immunohistochemistry for βGal in the somatosensory cortex. Scale bar, 50 μm. **(C-F)** Stereological quantification of cells expressing the immediate-early gene *c-Fos* (C, E) or βGal (D, F) in the somatosensory (C, D) or visual (E, F) reveals increased activity and SHH signaling in the somatosensory cortex, but not visual cortex. **(G)** Schematic depicting genetic strategy to label cells with temporally distinct SHH signaling (left panel) and timeline of experiment (right panel). In *Gli1*$^{nlacZ/+}$ mice, βGal expression labels cells with active SHH signaling. In *Gli1*^{CreER};Ai14 mice, Cre-mediated recombination promotes permanent expression of tdTom. In *Gli1*$^{CreER/nlacZ}$;Ai14 mice, tdTom expression identifies cells with SHH signaling at baseline (t_0) and βGal expression identifies SHH signaling in cells at the end of the experiment (t_1). Double labeled cells identify cells with persistent SHH signaling throughout the experiment. **(H-I)** Low power (H) and high power (I) images showing tdTom expression (magenta, left panel) and immunostaining for β-Gal (green, middle panel; merged image, right panel) in the cortex of mice housed in EE as described in (G). Scale bar, 250 μm. (I) Individual cells show those with upregulation (blue arrowhead), downregulation (open arrowhead) and persistent (white arrow) SHH activity. Scale bar, 50 μm. **(J-L)** The fraction of βGal-labeled cells that are single labeled (J), tdTom-labeled cells that are single labeled (K), and all cells that are double labeled (L) in SH or EE. Data points represent individual animals; bars show mean ± SEM; Welch's t-test.

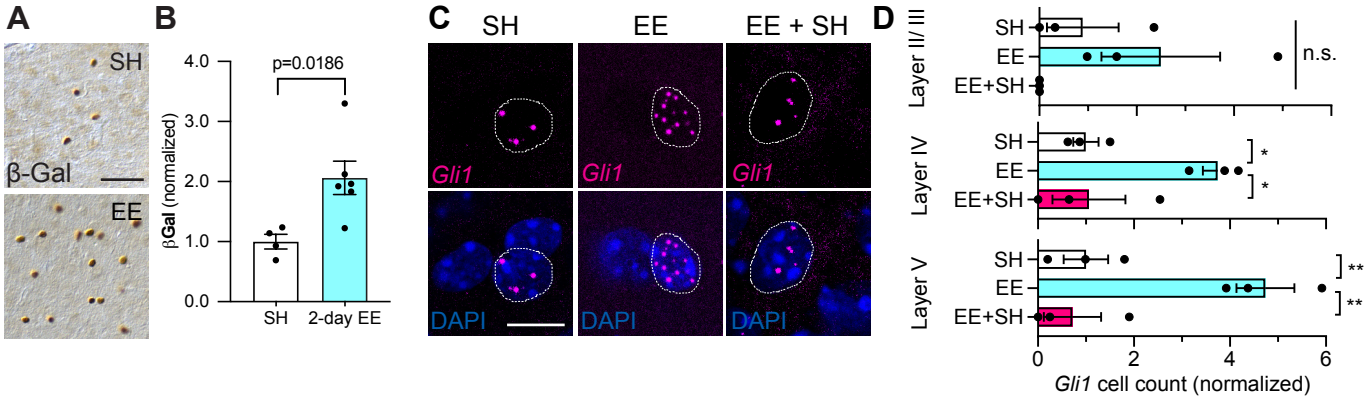

Figure 3. SHH signaling responds rapidly to sensory activation and is not persistent.
(A) Brightfield immunohistochemistry for β-Gal in the somatosensory cortex of *Gli1*$^{nlacZ/+}$ mice housed in SH (upper panel) or EE (lower panel) for 2 days. Scale bar, 50 μm. **(B)** Stereological quantification of β-Gal shows increased SHH activity in the somatosensory cortex after 2 days of EE. **(C)** Representative images of fluorescent *in situ* hybridization for *Gli1* mRNA in deep layers of the cortex from SH, EE, EE+SH housing conditions. Dotted line outlines individual DAPI nuclei with *Gli1* mRNA. Note the increase in *Gli1* transcripts in EE compared to SH. Scale bar, 10 μm. **(D)** Fraction of DAPI nuclei positive for *Gli1* mRNA in Layers II/ III, IV and V of the cortex from mice housed in SH or EE for 4 days or EE for 2 days followed by SH for 2 days (EE+SH). In each layer, at least 50 cells analyzed per animal. Data points represent individual animals; data represent mean ± SEM; Welch's t-test (B) and one-way ANOVA with multiple comparisons (D). Only p values <0.05 are shown. *p < 0.05, **p < 0.01, n.s. not significant.

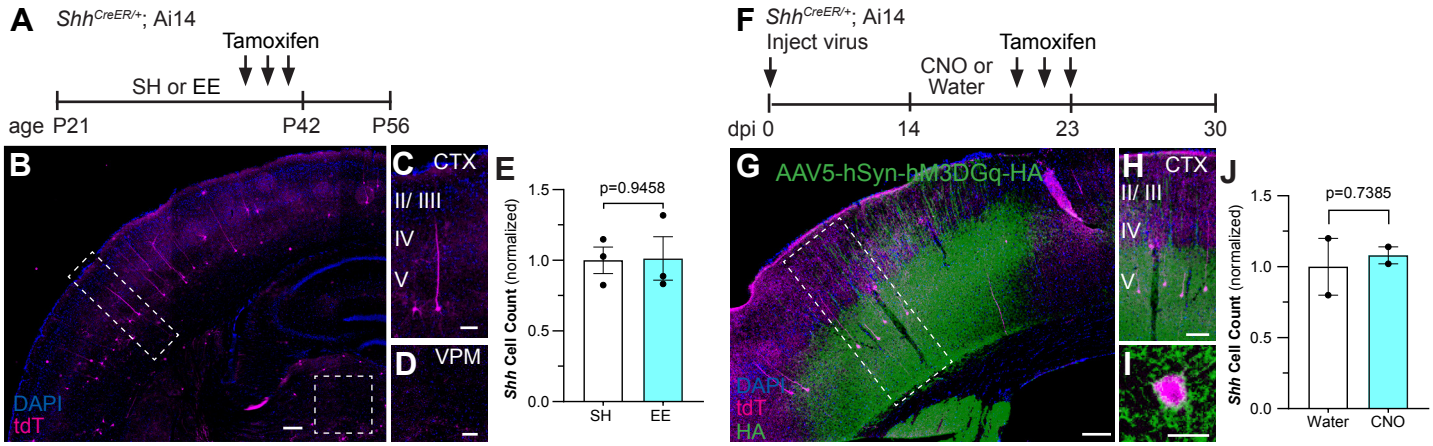

Figure 4. Sensory experience does not increase the number of *Shh*-expressing neurons.
(A) Schematic depicting experimental approach. P21 *Shh*$^{CreER/+}$; Ai14 mice were weaned into SH or EE cages at P21 and received 3 doses of tamoxifen from P39 - P41. Tissues were analyzed two weeks after the last tamoxifen dose. **(B-D)** Low power image showing tdTom labeled cells (magenta) in *Shh*$^{CreER/+}$; Ai14 mice. Labeled cells are found predominantly in layer V. Insets show individual cells with neuronal morphology in the cortex (C) and no labeled cells in the ventral posterior medial (VPM) nucleus of the thalamus (D). Counterstained with DAPI (blue). Scale bar, 25 µm. **(E)** The number of *Shh* neurons in the cortex in SH and EE mice. **(F)** *Shh*$^{CreER/+}$; Ai14 mice were injected with AAV5-hSyn-hM3DGq-HA targeting the somatosensory cortex. After 2 weeks, mice were fed CNO-medicated or unmedicated water for 10 days, receiving 3 doses of tamoxifen during the last 3 days. Tissues were analyzed seven days later. dpi, days post injection. **(G-I)** Immunolabeling for HA (green) shows the transduced region overlapping with tdTom labeled (magenta) cells in the cortex. Inset shown in (H). Individual cell shown at high power in (I). Scale bar, 25 µm. **(J)** The number of *Shh* neurons in the cortex between water control versus CNO. Data points represent individual animals; bars show mean ± SEM; Welch's t-tests.

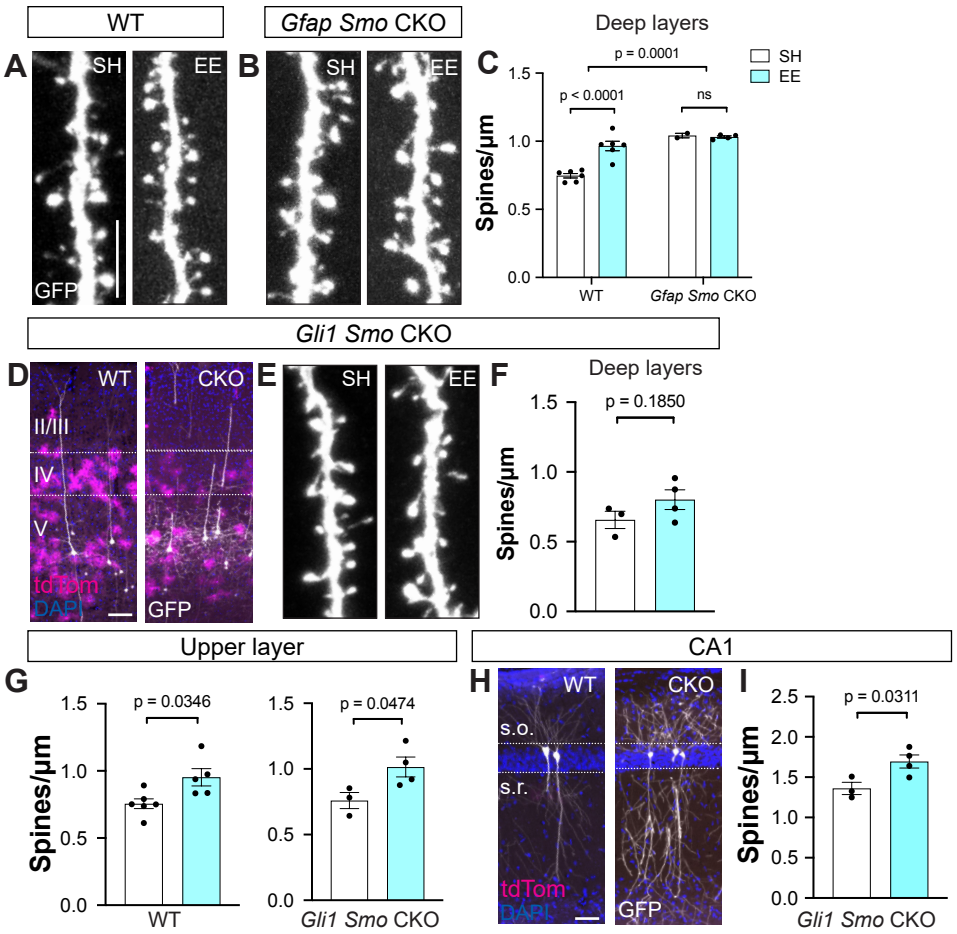

Figure 5. Experience-dependent structural plasticity requires SHH signaling.

(A-B) Representative dendritic segments in deep layers of WT (A) and *Gfap Smo* CKO (B) mice housed in SH or EE. Scale bar, 5 µm. **(C)** Spine density of dendritic segments in deep layers of WT and *Gfap Smo* CKO mice housed in SH or EE. **(D)** tdTom (magenta) labeled astrocytes and GFP (white) labeled neurons in the cortex of WT (C) and *Gli1 Smo* CKO (D) mice. Scale bar, 100 µm. **(E)** Dendritic segments from *Gli1 Smo* CKO mice housed in SH or EE. **(F)** Spine density of dendritic segments in deep layers is shown. **(G)** Spine density of upper layer dendritic segments from WT (left) and *Gli1 Smo* CKO (right) mice. **(H)** tdTom (magenta) and GFP (white) labeled cells in area CA1 of the hippocampus from WT and *Gli1 Smo* CKO mice, counterstained with DAPI (blue). Area CA1 contains few tdTom labeled cells reflecting the absence of Shh activity in hippocampal astrocytes. Scale bar, 50 µm. **(I)** Spine density from apical dendrites of CA1 neurons in *Gli1 Smo* CKO mice housed in SH or EE. Data points represent individual animals, bars show mean ± SEM, $n \geq 3 - 5$ dendritic segments analyzed per animal. Statistical testing performed by two-way ANOVA or Welch's t-test. s.o., stratum oriens; s.r., stratum radiatum.

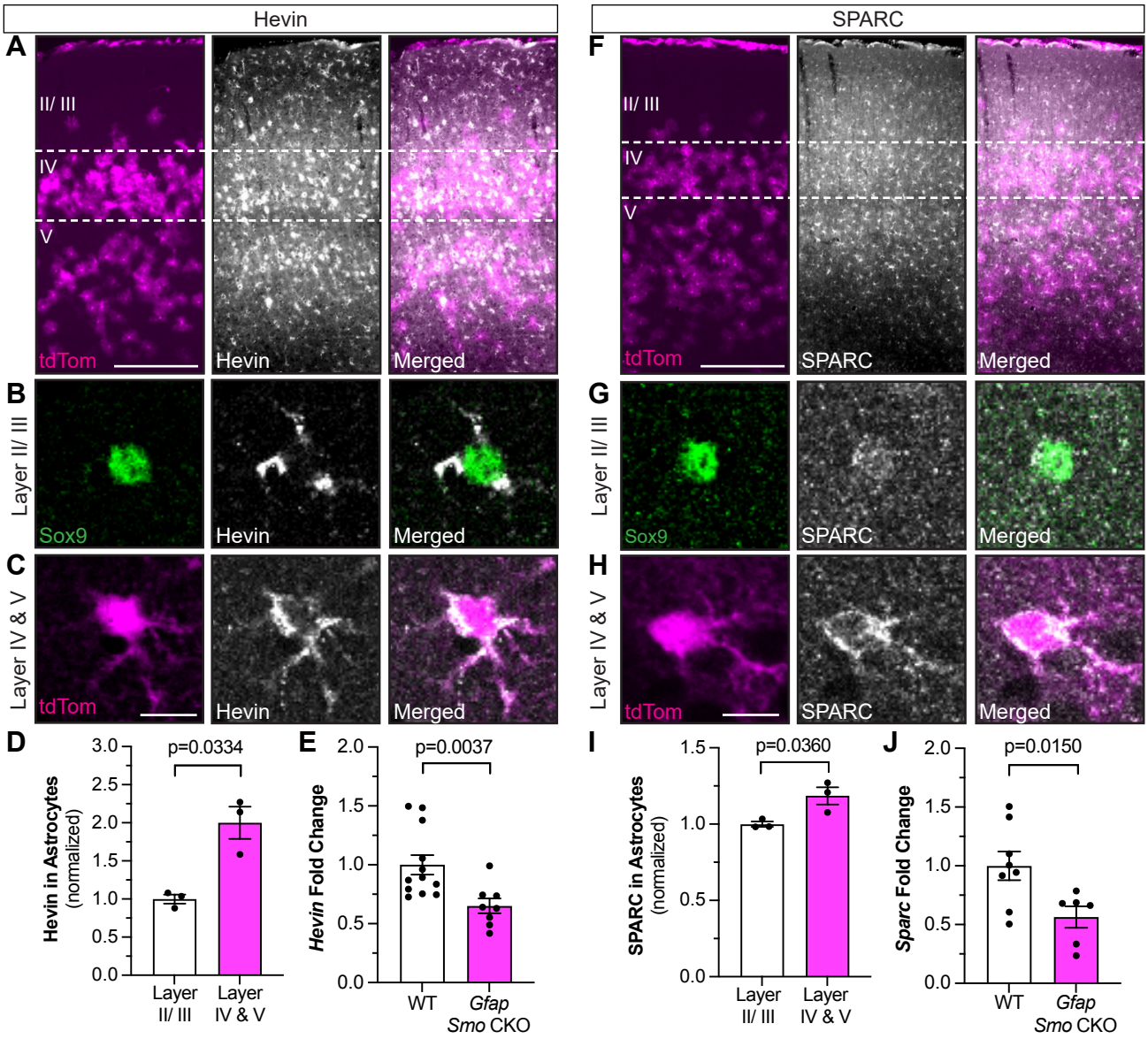

Figure 6. SHH signaling regulates expression of astrocyte-derived synapse-modifying cues Hevin and SPARC.

(A, F) Low power images of the cortex from *Gli1*$^{CreER/+}$; Ai14 showing tdTom cells (magenta, left panels) localized primarily in deep layers and immunofluorescent staining for Hevin (A, gray) and SPARC (F, gray) (middle panels) shows that Hevin and SPARC are enriched in deep layer astrocytes. Merged images in right panels. (**B-C, G-H**) Individual cells from upper layer (Layer II/ III) labeled with Sox9 (green, B, G) and deep layers (Layers IV & V) labeled with tdTom (magenta, C, H). Scale bar, 10 µm. **(D, I)** Single cell analysis of fluorescence intensity of Hevin (D) and SPARC (I) immunostaining in upper and deep layer astrocytes. *n=3* animals, 50 cells analyzed per animal. **(E, J)** qPCR for *Hevin* (E) or *Sparc* (J) expression in WT vs *Gfap Smo* CKO mice. *Hevin* and *Sparc* expression are significantly lower in CKO mice compared to WT controls. *n=13* WT mice, *n=8 Gfap Smo* CKO. Data points represent individual animals; bars show mean ± SEM; Welch's t-tests.

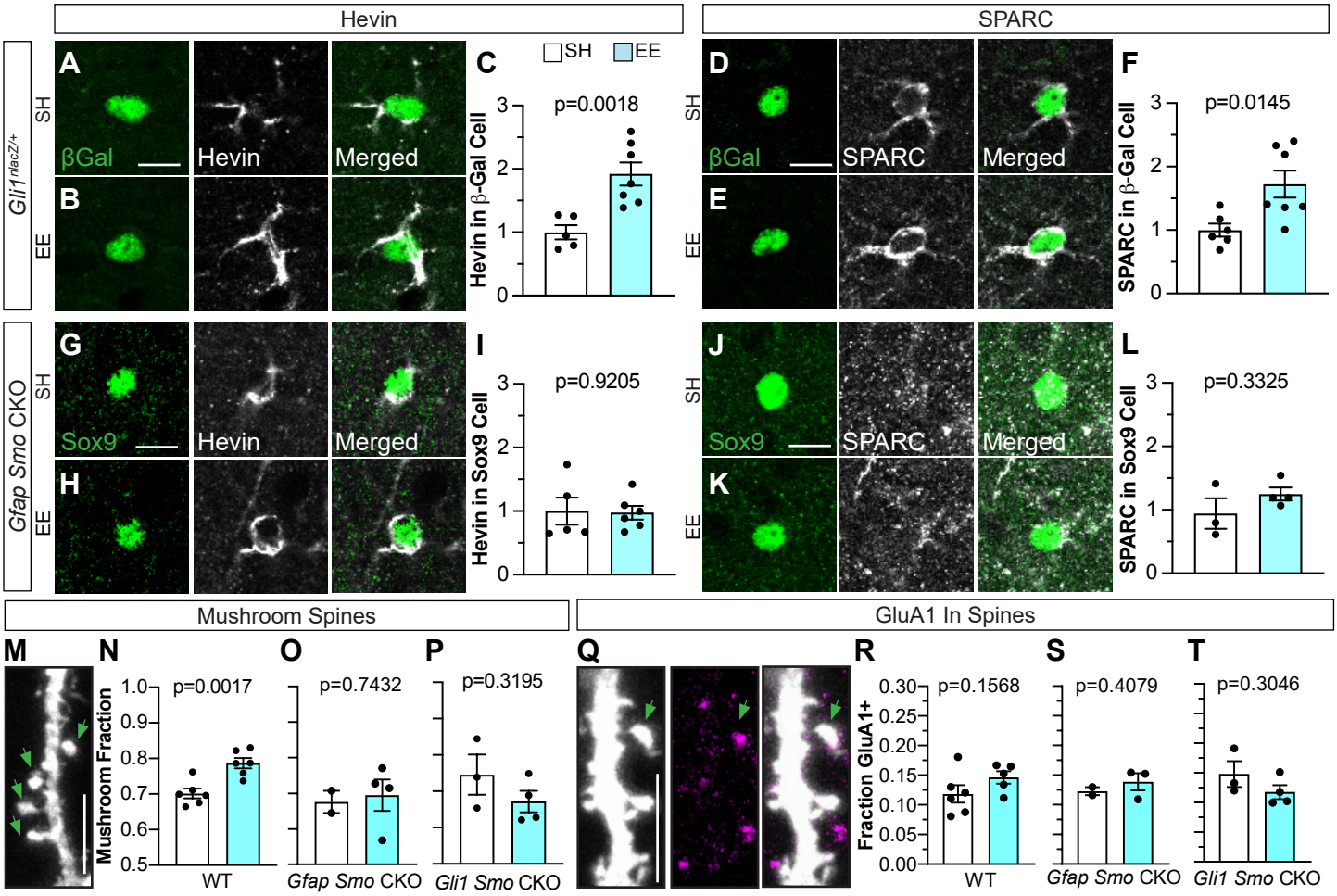

Figure 7. Experience-dependent Hevin and SPARC are SHH-dependent.
(A-B, D-E) Immunofluorescent staining for βGal (green, left panels, A, B, D, E) and Hevin (gray, middle panels, A, B) or SPARC (middle panels, D, E) in *Gli1*$^{nlacZ/+}$ mice housed in SH vs EE. Merged images in right panels. Scale bar, 10 μm. **(C, F)** Single cell analysis of Hevin (C) or SPARC (F) fluorescent intensity in βGal-labeled cells. *n=5-6* mice in SH, *n=7* mice in EE, 50 cells analyzed per animal. **(G-H, J-K)** Immunostaining for Sox9 (green, left panels, G, H, J, K) and Hevin (gray, middle panels, G, H) or SPARC (gray, middle panels, J, K) in *Gfap Smo* CKO mice housed in SH vs EE. Merged images in right panels. Scale bar, 10 μm. **(I, L)** Single cell analysis of Hevin (I) or SPARC (L) fluorescent intensity in Sox9-labeled astrocytes. *n=3-5* mice in SH, *n=4-6* mice in EE, 25 cells analyzed per animal. Scale bar, 10 μm. **(M)** Representative examples of protrusions categorized as mushroom spines (arrows). Scale bar, 5 μm. **(N-P)** Fraction of mushroom spines from WT (N), *Gfap Smo* CKO (O) and *Gli1 Smo* CKO (P) mice after SH vs EE. *n=2-6* mice from SH, *n=4-6* mice from EE, at least 300 spines from 3 dendritic segments analyzed per animal. **(Q)** Immunostaining for GluA1 (magenta) in dendritic spines. Arrow points to spine colocalizing with GluA1 puncta. Scale bar, 5 μm. **(R-T)** The fraction of GluA1+ protrusions in WT (R), *Gfap Smo* CKO (S) and *Gli1 Smo* CKO (T) mice after SH or EE. *n=2-6* mice in SH, *n=3-5* mice in EE, at least 200 spines analyzed per animal. Data points represent individual animals; bars show mean ± SEM; Welch's t-tests.